arXiv:astro-ph/0403211 v2 23 Mar 2004

Scheduled to appear in the Astronomical Journal, Vol 127, n.6, 2004 June

The nature of the mid-infrared population from optical identifications of the ELAIS-S1 sample

F. La Franca[1], C. Gruppioni[2], I. Matute[1], F. Pozzi[2,3], C. Lari[4], M. Mignoli[2], G. Zamorani[2], D.M. Alexander[5], F. Cocchia[6], L. Danese[7], A. Franceschini[8], P. Héraudeau[9], J.K. Kotilainen[10], M.J.D. Linden-Vørnle[11], S. Oliver[12], M. Rowan-Robinson[13], S. Serjeant[14], L. Spinoglio[15] & A. Verma[16]

ABSTRACT

We present a multi-wavelength catalog (15 μm, R, K-band, 1.4 GHz flux) plus spectroscopic identifications for 406 15 μm sources detected in the European Large Area *ISO* Survey (ELAIS) region S1, over the flux density range $0.5<S_{15\mu\mathrm{m}}<150$ mJy. 332 ($\sim$82%) sources are optically identified down to R$\sim$23.0. Spectra or bona fide stellar identifications are obtained for 290 objects ($\sim$88% of the optically identified sources). The areal coverage, mid-infrared (MIR) and optical completeness of the sample are discussed in order to allow statistical and evolutionary analyses. Two main spectroscopic classes have been found to dominate the MIR extragalactic population: $z < 0.5$ star-forming galaxies (from absorbed to extreme starbursts: $\nu L_\nu(15\mu\mathrm{m}) \approx 10^8 - 10^{11}$ L$_\odot$), which account for $\sim$75% of the sources, and Active Galactic Nuclei (AGN; both type 1 and 2), which account for $\sim$25% of the sources. About 20% of the extragalactic sources are dust-enshrouded starburst galaxies [e(a) spectra], and all the starburst galaxies appear more dust

[1]Dipartimento di Fisica, Università degli Studi "Roma Tre", Via della Vasca Navale 84, I-00146 Roma, Italy.

[2]INAF, Osservatorio Astronomico di Bologna, Via Ranzani 1, I-40127 Bologna, Italy

[3]Dipartimento di Astronomia, Università di Bologna, Via Ranzani 1, I-40127 Bologna, Italy

[4]INAF-CNR, Istituto di RadioAstronomia (IRA), via Gobetti 101, I-40129, Bologna, Italy

[5]Institute of Astronomy, Madingley Road, Cambridge, CB3 OHA, UK

[6]INAF, Osservatorio Astronomico di Roma, Via Frascati 33, Monteporzio-Catone, I-00040, Italy

[7]SISSA, International School for Advanced Studies, Via Beirut 2-4, 34014 Trieste, Italy

[8]Dipartimento di Astronomia, Università di Padova, vicolo dell'Osservatorio 5, I-35122, Padova, Italy

[9]Kapteyn Astronomical Institute, Landleven 12, 9747 AD Groeningen, The Netherlands

[10]Tuorla Observatory, University of Turku, Väisäläntie 20, FIN-21500, Piikkiö, Finland

[11]Niels Bohr Institute for Astronomy, Physics and Geophysics, Astronomical Observatory, Juliane Maries Vej 30, DK-2100 Copenaghen, Denmark

[12]Astronomy Centre, Department of Physics & Astronomy, University of Sussex, Brighton, BN1 9QJ, UK

[13]Astrophysics Group, Blackett Laboratory, Imperial College of Science and Technology & Medicine (ICSTM), Prince Consort Rd., London, SW7 2BZ, UK

[14]Centre for Astrophysics and Planetary Sciences, School of Physical Sciences, University of Kent, Canterbury, Kent CT2 7NR, UK

[15]INAF-CNR, Istituto di Fisica dello Spazio Interplanetario, Via del Fosso del Cavaliere 100, 00133 Roma, Italy

[16]Max-Planck-Institut für extraterrestrische Physics, Postfach 1603, 85740 Garching, Germany

extincted in the optical than nearby normal galaxies. We also identified 91 stellar objects (∼22% of the MIR sources). The counts for starburst galaxies and AGN down to 0.6 mJy have been derived. A general trend is found in the optical-MIR spectral energy distribution (SED) of the galaxies, where the MIR-luminous objects have larger MIR to optical luminosity ratios. Based on a variety of analyses, we suggest that the ELAIS sources fainter than R∼23 are luminous and ultra-luminous MIR galaxies (LIG-ULIGs; $\nu L_\nu(15\mu\mathrm{m})=10^{11}$-$10^{12}$ $\mathrm{L}_\odot$) at intermediate redshifts (z=0.5–1.5), and that consequently the present sample is virtually 100% spectroscopically complete up to z=0.5.

Subject headings: Cosmology: observations; Galaxies: distances and redshift; Galaxies: evolution; Galaxies: active; Galaxies: starburst; Infrared: galaxies

1. Introduction

The ISOCAM instrument (Cesarsky et al. 1996) on board of the *Infrared Space Observatory* (*ISO*; Kessler et al. 1996) has been able to unveil at 15 μm a population of MIR galaxies with two orders of magnitude fainter flux densities than observed by the *Infrared Astronomical Satellite* (*IRAS*). These galaxies result to be ten times more numerous than expected if there were no evolution from $z = 0$ up to $z = 1 - 1.5$ (see Elbaz et al. 1999). These results are confirmed by the detection of a substantial diffuse cosmic Infrared Background in the 140 μm - 1 mm range (Puget et al. 1996; Hauser et al. 1998; Fixsen et al. 1998; Lagache et al. 1999), which suggests a strong evolution of the galaxies in the IR (stronger than observed at any other wavelengths). The suggested evolution can either imply a larger fraction of galaxies experiencing an IR luminous phase in the past, or that MIR galaxies were more luminous in the past (see e.g. Chary & Elbaz 2001).

So far, the nature of the sources responsible for the strong evolution observed in the MIR band has only been studied in small fields, containing sources well known at other wavelengths: the Hubble Deep Field North (HDF-N; Aussel et al. 1999a,b) and South (HDF-S; Oliver et al. 2002; Mann et al. 2002; Franceschini et al. 2003), the Canada-France Redshift Survey (CFRS) 1452+52 field (Flores et al. 1999) and the ELAIS-S2 field (Pozzi et al. 2003). This has yielded a small but meaningful sample of sources sufficient for most multiwavelength studies. Most of these sources can easily be identified with relatively bright optical counterparts ($I < 22.5$) with a median redshift of $z \simeq 0.7-0.8$ imposed by the MIR k-correction (Aussel et al. 1999a,b; Flores et al. 1999).

However, to obtain reliable source counts and statistically significant information about the nature and evolution of the MIR extragalactic source population, large-area surveys covering a wide range of flux densities are required. In particular, it is very important to bridge the gap between the *IRAS* surveys ($S_{15\mu\mathrm{m}} > 200$ mJy) and the Deep ISOCAM surveys ($0.1 < S_{15\mu\mathrm{m}} < 2 - 3$ mJy). ELAIS (Oliver et al. 2000), with its broad flux range (0.5< $S_{15\mu\mathrm{m}}$ <150 mJy) and several thousand sources detected over a ∼12 deg^2 area (Rowan-Robinson et al. 2004), is the crucial survey to investigate the nature and evolution of the MIR sources in the region where the source counts start diverging from the non-evolution predictions (a few mJy at 15 μm; Elbaz et al. 1999; Gruppioni et al. 2002) and with data not affected by cosmic variance (which might be a strong effect in the narrow area surveys).

In order to better understand the nature of the MIR extragalactic population on the basis of a larger identification statistics than the ones obtained so far, we performed photometric and spectroscopic identifications for a source sample selected at 15 μm in the ELAIS southern field S1 (∼4 deg^2). Here we present the

results of the identification of 406 objects, which form a complete and highly reliable sub-sample drawn from the 15 μm catalog of Lari et al. (2001). The areal coverage, MIR and optical completeness are discussed in detail to allow statistical and evolutionary analyses with this sample. The counts down to 0.6 mJy for each class of source have been derived. The multiwavelength (radio, MIR, near-infrared (NIR), optical) properties of the 15 μm sources are investigated in order to study the nature and evolution of the infrared extragalactic population. The infrared luminosity function and the evolution of 15 μm galaxies and AGN are discussed in two companion papers (Pozzi et al. 2004; Matute et al. 2004, in preparation). A preliminary analysis of the AGN evolution has been presented in Matute et al. (2002) [17]

This paper is structured as follows: in section 2 we describe the 15 μm sample; in section 3 we present the optical CCD observations, the source identification and the cross-correlation with catalogs in other bands; in section 4 we describe the spectroscopic observations, the classification and the spectroscopic catalog; in section 5 we present the counts; in section 6 we discuss the nature of the MIR galaxies.

Throughout this paper we will assume $H_0 = 75$ km s^{-1} Mpc^{-1}, $\Omega_m = 0.3$ and $\Omega_\Lambda = 0.7$.

2. The ELAIS-S1 Mid-Infrared Sample

The primary *ISO* survey in the ELAIS regions was restricted to two bands: 15 μm (using ISOCAM), and 90 μm (using ISOPHOT; Lemke et al. 1996). Additional observations were performed in some parts of the survey area at 6.7 μm and 175 μm. The main survey area, consisting of $\sim$12 deg^2, is divided into four fields distributed across the sky in order to decrease the biases due to cosmic variance: three in the northern hemisphere (N1, N2 and N3) and one in the southern hemisphere (S1). Details of the survey can be found in Oliver et al. (2000). The final band merged catalog (6.7, 15, 90 and 175 μm) of the whole ELAIS survey is in Rowan-Robinson et al. (2003)[18].

The southern field, S1, centered at $\alpha(2000) = 00^h\ 34^m\ 44.4^s$, $\delta(2000)$ = -43° 28′ 12″, covers an area of the sky of about 2°×2°. In this field, a new method of data reduction (*LARI technique*), especially developed for the detection of faint sources, has been successfully applied, producing a catalog (complete at the 5σ level) of 462 sources in the flux density range 0.5 – 150 mJy[19]. Details about the data reduction technique and the source catalog have been presented in Lari et al. (2001)[20], while the sample completeness and the source counts at 15 μm obtained from that catalog have been presented and discussed by Gruppioni et al. (2002).

The whole S1 area has been surveyed in the radio with the Australia Telescope Compact Array down to $S_{1.4GHz} \simeq 0.4$ mJy (5σ, Gruppioni et al. 1999)[21]. The radio catalog in S1 consists of 652 sources detected at the 5σ level at 1.4 GHz. The radio-MIR correlation for starburst galaxies has been discussed by Gruppioni et al. (2003). About 40% the area has been observed by *BeppoSAX* down to a 2-10 keV sensitivity of $\sim 10^{-13}$ erg s^{-1} cm^{-2} by Alexander et al. (2001).

---

[17] A collection of papers and scientific results related to the ELAIS southern fields is available at http://www.fis.uniroma3.it/∼ELAIS_S.

[18] See http://astro.imperial.ac.uk/elais/.

[19] After flux corrections as explained at the end of §2.

[20] The catalog is available at http://www.bo.astro.it/∼elais/catalogs/ELAIS_CAM_15micron_S1.TAB.

[21] Available at http://www.bo.astro.it/∼elais/catalogs/ELAIS_RADIO_S1.TAB.

In this work we restricted our analysis to a highly reliable subsample of 406 sources out of a total 462 15 μm sources. The ELAIS-S1 area has been observed by ISOCAM at 15 μm with 9 separate rasters (see Figure 1). 20 out of the 462 sources were excluded as they were detected twice at the edges of overlapping rasters (in this case the sources with the highest S/N ratio have been selected). Moreover, 36 sources were excluded as we decided to use only those sources with the highest reliability (REL=0) after a visual inspection of their pixel histories. The ISOCAM observations of the central (S1_5) raster have been repeated three times (instead of one) and thus in this part the survey reaches fainter fluxes. As a consequence, we have divided the sample into two regions: a) S1_5 (i.e. raster 5) which covers 0.55 deg^2 and reaches a 20% completeness at $\sim$0.7 mJy, and b) S1_rest (i.e. all the remaining rasters) which covers 3.65 deg^2 and reaches a 20% completeness at $\sim$1.1 mJy. Note that in this work, as well as in the counts paper (Gruppioni et al. 2002), we used the 15 μm fluxes of the ELAIS-S1 sources reported by Lari et al. (2001), corrected following the detailed recipe described by Gruppioni et al. (2002). The completeness functions of the two regions as a function of the corrected 15 μm flux are shown in Figure 2 and are reported in Table 1, while the corrected 15 μm fluxes are reported in Table 2 and Table 3.

3. Optical photometry and multi-wavelength identifications

3.1. CCD Observations and Data Reduction

In order to obtain R-band optical photometry of the ELAIS-S1 region down to magnitudes fainter than the typical Schmidt plates limits (e.g. COSMOS[22]), we have carried out a CCD imaging campaign at the European Southern Observatory (ESO[23]). The whole S1 region has been covered by 168 overlapping CCD exposures obtained with DFOSC mounted on the 1.54 Danish/ESO telescope at La Silla (Chile). The observing runs were carried out during 12 nights (almost all photometric) during September 1996, October 1996 and September 1997. The CCD had 2052×2052 pixel array, with a pixel scale of 0.39″, and a field of view of 13.3×13.3 arc-minutes. The filter used was the Bessel R (ESO #452). About 97% the ELAIS-S1 area has been observed in the R-band (see Figure 1).

Photometric calibration was carried out by frequently observing (every $\sim$1-1.5 hours) the standard field stars "T Phe" ($\alpha(2000) = 00^h\ 27^m\ 49.0^s$, $\delta(2000)$ = -46° 48′ 02″; Landolt 1992). Those fields (about 10%) observed without photometric conditions were later calibrated using shorter integration images taken during photometric weather. Flat fields were obtained from blank fields in the sky at sunset and sunrise every night. The integration time for all science frames was 20 minutes. Standard data reduction was carried out with the MIDAS and IRAF reduction packages. Every science frame was subtracted for bias, and corrected for flat field.

Source searching on the final reduced images was carried out with SExtractor (Bertin & Arnouts 1996) The "MAG_BEST" source magnitudes have been used. The R-band magnitudes were computed after correction for airmass extinction, and without a color term, i.e. assuming a $V - R = 0$ color for all the objects. Due to the long observing campaign the characteristics of the CCD observations (e.g. seeing and magnitude limits) varied from field to field. The magnitude limits vary from 22.5 to 23.0 at 95% completeness level.

[22] http://xip.nrl.navy.mil/www_rsearch/RS_form.html.

[23] http://www.eso.org.

The astrometry has been computed by using the USNO2 catalog[24] as reference, with an internal accuracy of 0.26″ (rms), and an absolute radial accuracy (compared to USNO2) of 0.38″ (rms).

3.2. Identification of the 15 μm Sources in the R band

For the optical identifications of the ISOCAM sources we used the R magnitudes and positions given in the CCD catalog. Ten sources were not observed by the CCD imaging. For 7 out of these 10 sources the R-band USNO2 magnitudes have been used. The remaining 3 sources (ELAISC15_J003559-430232, ELAISC15_J003912-442051, ELAISC15_J004023-433459) have to be considered fainter than R=20 (see Table 2). Two sources (ELAISC15_J003034-433428 and ELAISC15_J003857-431719) were too close to bright stars and the optical identification was not possible. To estimate the identification reliability, we adopted the likelihood ratio technique as described by Sutherland & Saunders (1992) (see Ciliegi et al. (2003) for a detailed description). When possible counterparts fainter than R=23.0 were found, the identifications were not statistically discussed, and presented only as tentative. Taking into account all of the optical identifications, 332 (∼82%) out of the 406 ELAIS-S1 sources have a reliable counterpart down to R∼23 (only 7 sources have 23.0<R<24.3), 2 are impossible to identify, and 72 (∼18%) are to be considered fainter than R∼23.0 (see Figure 3). In the following we will call these sources "EMPTY".

3.3. K band and 1.4 GHz identifications

The sample has been cross-correlated with the K-band catalog from the Two Micron All Sky Survey[25] (2MASS), which reaches a K-band limit of ∼15.6 (at 95% completeness level). In total 211 sources have been detected in the K-band. Since the whole S1 field has been surveyed in the radio (1.4 GHz) with the Australia Telescope Compact Array to an average 1σ level of 0.08 mJy (Gruppioni et al. 1999), at each ISOCAM position, we have searched for detection in the radio map down to 3 σ, finding 71 likely radio counterparts (61 with measured redshifts; see Gruppioni et al. 2003 for details). The results of the multi-band identifications are reported in Table 2.

4. The spectroscopic catalog

4.1. Spectroscopic observations

Spectroscopic observations of the optical counterparts of the ISOCAM S1 sources were carried out at the 2dF/AAT and ESO Danish 1.5-m, 3.6-m and NTT telescopes during September and October 1998, September and November 2001, September and October 2002. A total of 15 ESO nights and 2 UK (from the Panel for the Allocation of Telescope Time; PATT) nights were allocated.

The 2dF/AAT multifiber feed spectrograph was used with 200 fibers equipped with the 300B grism and the remaining 200 fibers with the 270R grism (about 10 Å instrumental resolution). Because of poor weather conditions only half an hour of integration was possible during each night, reaching a magnitude

[24] http://www.nofs.navy.mil/.

[25] See http://www.ipac.caltech.edu/2mass.

limit of R∼19.5. The ESO spectrographs (DFOSC, EFOSC2 and EMMI) were all used in single slit low resolution mode (10-20 Å resolution) in the wavelength range 3500-9500 Å, and reaching an average S/N ratio per resolution element of ∼15-30 in the wavelength range 4000-7000 Å. The reduction process used standard MIDAS and IRAF facilities. The raw data were sky-subtracted and corrected for pixel-to-pixel variations by division with a suitably normalized exposure of the spectrum of an incandescent source (flat field). Wavelength calibrations were carried out by comparison with exposures of He, Ar and Ne lamps. Relative flux calibration was carried out by observations of spectrophotometric standard stars (Oke 1990, Hamuy 1992, 1994).

4.2. Classification

We have spectroscopically classified 290 (∼87%) out of the 332 sources optically identified (∼71% of the whole 15 μm sample). The sample has been cross-correlated with the TYCHO2 (Høg et al. 2000) and NED[26] catalogs in order to identify known stars and extragalactic objects. Sixty-two TYCHO2 stars were found. The remaining objects brighter than R=15 were visually inspected in the R band images and those suspected to be extended/extragalactic were spectroscopically observed. Fifteen sources with R<15 were considered to be bona fide stars on the basis of the visual inspection, while 14 were spectroscopically identified as stars at the telescope. In total we found 91 stars (all of them brighter than R=15) and 199 extragalactic sources.

In order to classify the extragalactic sources we have first identified type 1 AGN (AGN1) when permitted lines with rest frame full width half maximum (FWHM) larger than 1200 Km/s were found. The remaining objects were classified according to two methods.

The first method was used to identify type 2 AGN (AGN2), and to separate them from other emission line galaxies such as HII/starburst and Low Ionization Narrow Emission Regions (LINER). All the objects with narrow Hβ or [OIII]λ5007 emission lines having EW (measured as the ratio between the integrated flux in the line, as resulting from a gaussian fit, and the flux of the continuum at the line wavelength) larger than ∼3-5Å (our line detection limit), were classified according to three diagnostic diagrams: 1) [OIII]λ5007/Hβ ratio versus [NII]λ6583/Hα ratio; 2) [OIII]λ5007/Hβ ratio versus [SII]λ6725/Hα ratio; 3) [OIII]λ5007/Hβ ratio versus [OII]λ3727/Hβ ratio (e.g. Veilleux & Osterbrock 1987; Tresse et al. 1996; see Figure 4 for an example). The Hα and [NII]λ6583 lines were deblended using the IRAF task `splot`, which assumes Gaussian line profiles and a linear background.

The above method is efficient in separating AGN from starburst activity, but does not provide information on the nature of a large fraction of our galaxies, which do not show [OIII] and Hβ emission lines. We have thus applied the classification scheme of Dressler et al. (1999) (see also Poggianti et al. 1999 and Poggianti & Wu 2000) to all the "non AGN" galaxies. This method is based primarily on two lines, [OII]λ3727 in emission and Hδ in absorption, which are good indicators of (respectively) current and recent star formation (SF) in distant galaxy spectra. Under this scheme the spectra have been divided in:

1. e(a) (having 3Å<EW([OII])<40Å and EW(Hδ)≥4Å), spectra of dust-enshrouded starburst galaxies;
2. e(b) (having EW([OII])>40Å), spectra with very strong emission lines of galaxies which are undergoing strong star formation;

[26] See http://nedwww.ipac.caltech.edu/.

3. e(c) (having 3Å<EW([OII])<40Å and EW(Hδ)<4Å), typical spectra of spirals which have been forming stars in a continuous fashion;

4. k (absent [OII] and EW(Hδ)<3Å), spectra of passive elliptical-like galaxies with neither ongoing nor recent star formation;

5. k+a/a+k (absent [OII] and EW(Hδ)$\geq$3Å), spectra of poststarburst galaxies with no current star formation which were forming stars at a vigorous rate in the recent past (last 1.5 Gyr).

6. k(e), spectra similar to the k-type but with signs of at least one emission line. This class was introduced by us following Duc et al. (2002).

Following this classification, we found 25 AGN1, 23 AGN2, 37 e(a), 11 e(b), 68 e(c), 32 k(e) and 3 k galaxies. No k+a/a+k galaxy was found. Thirteen objects could not be classified on the basis of this scheme because the wavelength range of [OII] and Hδ lines was not observed (they were observed with the red grism of the 2dF spectrograph). Two of them were classified e(b) (starburst) galaxies according to the [OIII]λ5007/Hβ and [NII]λ6583/Hα ratios, while the remaining 11 galaxies were classified k(e) because no [OIII]λ5007 and Hβ line was detected, while the Hα emission line was present. In Figure 5 we show the composite spectra of each type of galaxy found under this classification scheme.

We should stress that the number of identified AGN2 has to be considered a lower limit. *XMM* and *Chandra* surveys have revealed significant numbers of (mostly absorbed) AGN with L(2-10 keV)$>10^{42}$ erg s^{-1} (i.e. AGN2) whose optical spectra do not show sign of AGN activity (see e.g. Fiore et al. 2000; 2003). Recent (June-July 2003), 100 Ksec long, *XMM* observations of S1-5 have revealed indeed that about 10-20% of the counterparts of our *ISO* sources classified as no-AGN galaxies on the basis of their optical spectra, can harbor an X-ray emitting AGN (the *BeppoSAX* observations presented in Alexander et al. (2001) are too shallow to provide tighter AGN constraints). Under the reasonable assumption that all these objects are AGN2, the number of AGN2 in the ELAIS-S1 sample should be increased by at least a factor of 2. A more detailed discussion on the X-ray/MIR relationship of AGN and starburst galaxies is beyond the scope of this paper and will be presented by La Franca et al. (in preparation).

In Table 2 we list the multiband associations to the 15 μm sources with the likelihood and reliability of the R band identifications, plus the redshift, the spectroscopic classification and the νL_ν luminosities at 15 μm and in the R-band. In Table 3 we present the line measurements of the spectra which include the calcium break (D_{4000}; measured from the fluxes in the intervals 3750-3950 Å and 4050-4250 Å; see Dressler et al. 1999) and the EW for the [OII]λ3727, Hδ, Hβ, [OIII]λ5007, Hα, [NII]λ6583 and [SII]λ6725 lines (positive values correspond to absorption lines).

Figure 6 shows the distribution of the 211 ELAIS-S1 sources detected both in the R and K bands, in the $R-K$ versus $R-mag15$ plane, where we have defined $mag15 = -2.5log(S_{15}(mJy))$. This diagram shows a clear separation of the locus of the stars from the locus of the galaxies: for any given $R-K$ color, stars populate a region with a two order of magnitude lower MIR to optical luminosity ratio. Note that only one early-type galaxy and two stars are located in the intermediate area of the diagram between those occupied by stars and galaxies. This means that stars can easily be separated from galaxies based purely on their infrared to optical flux ratio (see also Väisänen et al. 2002).

4.3. Completeness

The S1_5 area is 99% spectroscopically complete (72/73) down to R=21.6. The S1_rest area is 97% (216/222) complete down to R=20.5 (see Figures 7 and 8). These magnitude limits have been used for the statistical analysis of the evolution of AGNs and galaxies by Matute et al. (in preparation) and Pozzi et al. (2004) respectively. Both Figures 7 and 8 show a separation between stars and galaxies, the stars being optically brighter than galaxies, and also the appearance of a separate population of galaxies at faint magnitudes ($R > 20$). See §6.3 for a detailed discussion on this point.

In the following we will call *noIDs* all the 116 ELAIS-S1 sources which are without spectroscopic identification (i.e., including also 72 EMPTY sources and 2 sources with no optical identification becouse too close to bright stars; see §3.2).

5. Counts and contribution to the MIR background

We have computed the contribution of each class of sources to the 15 μm source counts in the mJy flux region. The integral counts for star-forming galaxies and AGNs (as defined on the basis of the optical spectra) are reported in table 4 (see Figure 9). As already discussed in section §4.2, the counts of AGN should be considered as lower limits. All ELAIS-S1 extragalactic sources (including the *noIDs*), with 15 μm fluxes brighter than 0.6 mJy, produce a 15 μm background of νI(ν) = 0.34 nW m^{-2}sr^{-1}. This corresponds to ∼12% of the total extragalactic background estimated by Metcalfe et al. (2003) of νI(ν)=2.7 nW m^{-2} sr^{-1}.

The sources spectroscopically identified with galaxies (no AGN) produce a flux of νI(ν)=0.16 nW m^{-2} sr^{-1}. The empty fields (mainly objects fainter than R∼23) produce νI(ν)=0.14 nW m^{-2} sr^{-1}, while the AGNs produce νI(ν)=0.04 nW m^{-2} sr^{-1}. If we assume that the *noID* sources correspond mainly to starburst galaxies, we derive a ∼90% contribution of starburst galaxies and a ∼10% contribution of AGNs to the 15 μm background at fluxes brighter than 0.6 mJy. If our preliminary estimate of the fraction of of hidden X-ray emitting AGN2 among the galaxies is taken into account, these figures may well be consistent with the higher estimates (∼15–20%) for the contribution of AGN derived by Alexander et al. (2002), and Fadda et al. (2002).

6. Nature of the 15 μm extragalactic source population

6.1. Redshifts and luminosities

In Figure 10 the redshift distribution of the spectroscopically identified sources is shown. While AGN1 reach redshifts up to z∼3, all AGN2 and galaxies have redshifts lower than 1, with an average of $<z>\sim 0.3$. A possible hint of structure at $z \sim 0.15$ and $z \sim 0.20$ is present.

We computed the νL_ν luminosities of our sources at 15 μm (L_{15}) and in the R-band (L_R). For each class of objects a K-correction was applied according to the spectral classification (see Figure 11). In the infrared the K-corrections were based on: a) the SED from Elvis et al. (1994) for AGN1, b) the SED of NGC1068 for AGN2 (Sturm et al. 2000) and, c) the SED of M82 for all of the remaining sources, except the absorption line galaxies (for which M51 was considered). In the optical, the K-correction from Natali et al. (1997) was used for AGN1, while for AGN2 the K-corrections were computed by using the average of our

corresponding optical spectra. For the galaxies the SEDs of M82 and M51 were used, consistently with what has been done for the 15 μm flux. The model SEDs of both M82 and M51 were taken from the GRASIL[27] library of models (Silva et al. 1998). For M82, the MIR (5 – 18 μm) has been replaced with the observed ISOCAM CVF spectrum (Förster Schreiber et al. 2003).

In Figure 12 the L_{15} luminosities are shown as a function of redshift. A luminosity dependence of the classes of objects is evident. AGN1 are the most luminous and most distant sources with $< logL_{15} > \sim 12.1$, while AGN2 are less luminous and less distant with $< logL_{15} > \sim 10.6$. Finally, the least luminous and least distant sources are the galaxies with $< logL_{15} > \sim 9.9$.

6.2. The optical-MIR SED of starburst galaxies

In Figure 13, L_{15}/L_R versus L_{15} is shown for all of the ELAIS-S1 15 μm galaxies plus sources from the spectroscopic identifications in the HDF-S from Franceschini et al. (2003), the HDF-N (ISOCAM data from Aussel et al. 1999; spectroscopic data from Cohen et al. 2000; magnitudes from Hogg et al. 2000), and the local sample of *IRAS* 12-μm galaxies of Rush, Malkan & Spinoglio (1993; RMS; after conversion to 15 μm by using the M51 and M82 SED for normal and starburst galaxies respectively). A clear relation which is valid for all of the considered surveys is found, although it involves only objects with optical identification. The best fit to the data is

$$log(L_{15}/L_R) = 0.47 log L_{15}[L_\odot] - 5.02.$$

The 1σ dispersion of the relation is 0.32. Note that type 1 AGN have been excluded because of the different mechanism responsible for their luminosities, placing them on a different L_{15}/L_R versus L_{15} plane location with respect to galaxies. On the contrary, type 2 AGN follow the same relation as all the other galaxies. This relation implies that the average optical-IR spectral energy distribution of galaxies is luminosity dependent, with more luminous galaxies having larger L_{15}/L_R ratios. A two order of magnitude increase in luminosity implies a 10 times larger L_{15}/L_R ratio. This relation is also discussed and taken into account for the analyses of the evolution of starburst galaxies and AGNs presented in two companion papers by Pozzi et al. (2004) and Matute et al. (in preparation).

6.3. The nature of the sources fainter than the spectroscopic or photometric limits

As already shown by Gruppioni et al. (2002), the 15-μm extragalactic counts show an upturn at fluxes fainter than $\sim$1 my (see also Elbaz et al. 1999), which is interpreted as due to the contribution of the strong cosmological evolution of the starburst population. This interpretation is discussed in detail by Pozzi et al. (2004). Anyway the counts (see Figure 9) show that the upturn is mostly due to the contribution of the *noIDs* sources (i.e. sources fainter than our spectroscopic or photometric limits), which represent about half of the extragalactic sources at fluxes $\sim$0.6-1 mJy. These sources could be either optically less luminous (absorbed?) galaxies at redshift similar to those of the already spectroscopically identified sample, or higher redshift sources. We favor the second hypothesis on the basis of the following discussion.

We have tried to estimate a redshift for the *noIDs* sources in order to distinguish between the two different scenarios described above. We have combined our sample with the fainter HDF-S and HDF-N

[27] available at http://web.pd.astro.it/granato/grasil/modlib/modlib.html.

samples. Then we have tried to derive a flux-redshift relationship applicable to the ELAIS-S1 unidentified sources in order to estimate their redshifts. After several trials using multiple polynomial relations between $log(z)$ and both 15 μm flux ($logS_{15}$) and magnitude (R), we have assigned a redshift to the 116 $noIDS$ sources on the basis of their R magnitudes only ($R = 23$ was assumed for all the unidentified 76 ($EMPTY$) sources), by considering the following empirical relation and its spread:

$$log(z) = -6.350 + 0.443\ R - 0.007\ R^2 + G(0, \sigma_{rel}),$$

where σ_{rel} (= 0.15) is the 1σ dispersion of the relation and $G(0, \sigma_{rel})$ is a Gaussian distribution with center 0 and width σ_{rel} (see Figure 14, *Top*). Note that the fit is non-linear in $log(z)$ vs. R, since we found that a linear fit to the data extrapolated to faint magnitudes was providing too high redshifts, inconsistent with the k-correction limit of ISOCAM ($z \sim 1.5$) and with the median redshifts of $R = 24 - 25$ objects from the HDF-S and HDF-N. Using the estimated redshifts, we have computed MIR and optical luminosities for the unidentified sources (by assuming all of them being star-forming galaxies, thus using M82 SED) and we have placed also these objects in the L_{15}/L_R vs. L_{15} diagram (see the *bottom* panel of Figure 14).

According to our estimates, the unidentified objects in our survey are likely to be rather luminous MIR objects (L_{15} ranging between $\sim 10^{11}$ $L_\odot$ and a few 10^{12} $L_\odot$, in the LIG/ULIG region), and their optical and MIR estimated luminosities appear to be consistent with (and extending to higher luminosities) the L_{15}/L_R vs. L_{15} correlation found for the identified sources. The estimated redshift distribution for the unidentified sources is shown in Figure 15, where it is compared with the distribution found for the spectroscopically identified sources and with the model fitting derived from our data (i.e. the 15 μm luminosity function in S1; Pozzi et al. 2004). The agreement between the model and the data (either observed and estimated) is good. It results that the unidentified sources are expected to fill the secondary high-z peak of the model-predicted redshift distribution.

The double peaked redshift distribution (see Figure 15) is caused by the 15 μm k-correction. As shown in Figure 11, at z=0.5 the 15 μm observed fluxes decrease by ∼30%. For our flux limited sample this implies that the ELAIS-S1 galaxies at z=0.5 correspond to 30% higher intrinsic luminosities. But at z=0.5 the ELAIS-S1 galaxies sample the bright steep slope of the luminosity function ($\log(L_{15}) > 11 > L^*$), where 30% higher intrinsic luminosities correspond to an order of magnitude lower density of galaxies. This decrease of density of galaxies is also evident in the R-magnitude distribution (see Figures 7 and 8), where, due to the k-correction effects, a lack of sources with R∼20-21 (and z∼0.5) is evident. The R-band histogram (Figure 7) shows a triple peaked distribution: stars populate the brightest peak at R∼10-12, z<0.5 galaxies populate the intermediate peak at R∼17-19, and higher redshift (z>0.5) galaxies populate the fainter peak that can be observed at R>21-22.

Under the alternative hypothesis that ELAIS-S1 $noIDs$ were instead lower redshift (z<0.5) sources suffering from dust extinction, it would be more appropriate to consider the 15-μm flux – z relation rather than the $R - z$ relation (because affected by dust) to estimate their redshifts. In this case, we would obtain a redshift distribution for the $noIDs$ sources similar to that of the optically identified, but they would be located in a separate region of the L_{15}/L_R vs. L_{15} diagram (i.e. at similar L_{15}, but with at least one order of magnitude higher L_{15}/L_R). This would imply the existence of a absolutely different population of objects, with much higher level of obscuration (without continuity) than the identified ones, but at similar flux density and redshifts.

The first hypothesis is also supported by the faint spectroscopic identifications in the HDF-N (Aussel et al. 1999) and CFRS 1452+52 (Flores et al. 1999) fields which have mainly found a population of z=0.4-1.0

galaxies. For all these reasons we conclude that the vast majority of the faint (R>20.5) ELAIS-S1 *noIDs* objects should belong to the same population as the identified sources, but at higher redshifts (z=0.5-1.5), and that consequently the present sample is virtually spectroscopically complete up to z=0.5, as far as the star forming galaxies are concerned.

6.4. The nature of the MIR galaxies

As we have seen, our sample is virtually complete up to $z \simeq 0.5$. Up to this redshift we have identified 167 extragalactic objects: 3 AGN1, 20 AGN2, 33 e(a), 9 e(b), 67 e(c), 32 k(e), and 3 k galaxies. No k+a/a+k galaxy was found. The average redshift of the sample is $<z>$=0.20. The number of e(a) galaxies rises to 37 if we classify also the AGN2 according to the classification scheme of Dressler et al. (1999) (see §4.2). The majority of the sources with z<0.5 is composed by normal star forming spirals (e(c), 41%), and by absorbed star forming galaxies (e(a), 20%; 23% including the AGN2). The total fraction of optical spectra which show emission lines which are indicators of star formation (e(b)+e(c)+e(a)+k(e)) is 84%. 14% of the sources are AGNs, and only 2% of the sources do not show emission lines (k galaxies). This confirms that the MIR and the optical data agree on revealing both ongoing star formation and accretion driven (AGN) activities. The lack of k+a/a+k galaxies in the ELAIS-S1 sample suggest that these galaxies are not strong MIR emitters. This result is consistent with the lack of emission lines in their optical spectrum and with their post-starburst interpretation (see Poggianti and Wu 2002).

The e(a) galaxies are believed to be associated with dust enshrouded starburst galaxies. Following Poggianti et al. (1999) and Poggianti & Wu (2000), the spectra of e(a) galaxies are explained as the result of selective dust extinction which affects the youngest, most massive, stars in HII regions much more than the older stellar population responsible for the continuum flux. A search for similar spectra in the local universe (Poggianti et al. 1999) revealed that they are frequent among merging/strongly interacting galaxies (∼40%), while they are scarce in optically selected surveys of field galaxies at low z: 7-8% in the Las Campanas Redshift Survey and in Kennicut (1992). Dressler et al. (1999) and Poggianti et al. (1999) found that e(a) galaxies constitute about 10% of their sample of cluster and field galaxies at z∼0.4-0.5.

At 15 μm most (71%) of the sources with optical spectroscopy in the CFRS are classified as e(a) galaxies and have a mean redshift $<z>$=0.76, while at z=0.18, in the cluster of galaxies Abell 1869, Duc et al. (2002) find 25% of 15 μm galaxies classified as e(a).

The observed 20-23% fraction of e(a) galaxies in the ELAIS-S1 sample at $<z>$=0.20, is thus higher than observed in optically selected samples and in agreement with the estimates at similar redshifts by Duc et al. (2002) in a MIR selected sample. This confirms that e(a) galaxies are dusty absorbed star forming galaxies which are preferentially selected at longer wavelengths (MIR), and whose frequency increases with increasing redshift, as the cosmic star formation rate.

We have compared the $R-K$ colors of our sources to those of the field galaxies and we did not find evidences of reddening. Becouse of the bright K-band limit magnitude we limited our comparison in the magnitude range R=15-17.5, and consequently the statistic are poor. The average R-K color is 2.04 and 2.27 for ELAIS and field galaxies respectively, with a 1σ dispersion of ∼0.50 for both samples. On the contrary, dust extinction seems to affect the spectral lines of our objects. In figure 16 the EW of the [OII] line is compared to the EW of the Hα+[NII] line. The $EW([OII])/EW(H\alpha+[NII])$ ratio is related to the differential extinction due to dust, the $[OII]$ emission being more affected than $H\alpha$ emission due to its shorter wavelength. The dashed line in Figure 16 is the relation found by Kennicutt (1992) for local field galaxies

($EW([OII])/EW(H\alpha+[NII])$=0.4). Most of our sources lie below that relation, and the presence of upper limits (i.e. [OII] non-detections) would even lower the average value of the $EW([OII])/EW(H\alpha+[NII])$, implying a larger amount of extinction in our data than in the local sample of Kennicutt (1992). The average ratio for the galaxies having both [OII] and Hα+[NII] lines is 0.36±0.15, 0.35±0.03, 0.29±0.02 for e(b), e(c) and e(a) galaxies respectively. Thus, as expected, at least for the normal star forming (e(c)) and absorbed star forming (e(a)) galaxies the difference from the local observed ratio (0.4) is significant.

In order to disentangle a possible dependence on redshift or luminosity of the average extinction of the galaxies, we have combined our sample with a subsample of 39 galaxies from the local sample of RMS for which EW measures for [OII] and Hα+[NII] were available in the literature (see Alexander & Aussel (2000) for a discussion of this sample). The data show that the extinction affecting the lines is an increasing function of luminosity while a correlation with redshift is not statistically significant: a partial correlation Kendall test gives in fact a 10^{-4} probability that the EW is not dependent on luminosity, and a 0.04 probability that the EW is not dependent on redshift. Figure 17 (*top*) shows the distribution of the RMS and ELAIS galaxies in the luminosity-redshift plane. We have then selected the galaxies with 0.010<z<0.055 in order to show the dependence on luminosity (Figure 17, *middle*), and the galaxies in a small luminosity interval (9<$logL_{15}(L_{\odot})$<10) in order to show the not significant trend with the redshift (Figure 17, *bottom*). These results suggest an increase of dust extinction with luminosity. Similar results, based on a smaller sample, were found also by Pozzi et al. (2003) in one of the smaller but deeper ELAIS fields, S2.

A quantitative estimate of the amount of optical extinction affecting the ELAIS-S1 MIR galaxy sample can be obtained by the measure of the observed Balmer decrement in the Hα and Hβ lines. We have made this measure on two composite spectra for each class of galaxies: one including only spectra with detected Hα and Hβ emission lines, and one including also spectra with no detected Hβ line. Spectra showing Hβ lines in absorption were excluded. This method was adopted in order to minimize the effects of underling Hβ absorption which causes the observed Hα/Hβ ratio to be larger. For this reason the extinction estimates we derive have to be considered upper limits. In Table 5 our estimates in the case of B recombination with a density of 100 cm^{-3} and a temperature of 10000^{o}K (Osterbrock 1989) are shown. The higher values of E(B-V) were always obtained when the spectra without Hβ detection were included in the composite spectra. These values correspond to an extinction A_V=3.2×$E(B-V)$ of about 1.5, 3.5, 4.0, 4.5 mag for e(b), e(c), e(a) and k(e) galaxies respectively. These value refers to the absorption of the lines emission; typically the absorption on the continuum is a factor of two smaller (see also Pozzi et al. 2003, and Poggianti & Wu 2000 for similar results). As expected, the larger extinction values are found for e(a) and k(e) galaxies, reinforcing the interpretation that the e(a) signature is associated with dust extincted starbursts.

6.5. The star formation rate

We have estimated the star formation rate (SFR) of the ELAIS-S1 sources from their 15 μm infrared luminosity. The SFR estimator has been computed as:

$$SFR[M_{\odot}/yr] = 11.25 \times 10^{-23} L_{15}[WHz^{-1}],$$

assuming a Salpeter initial mass function (IMF, Salpeter 1955) between 0.1 and 100 $M_{\odot}$, a dependence of SFR from $L_{60\mu m}$ as given by Mann et al. (2002; $SFR[M_{\odot}/yr] = 0.9 \times 10^{-23} L_{60\mu m}[WHz^{-1}]$), and a mean value of the ratio $< L_{15\mu m}[WHz^{-1}]/L_{60\mu m}[WHz^{-1}] > \simeq 0.08$, typical of starburst galaxies such as M82.

In Figure 18 the SFRs as a function of redshift are shown. Type 1 AGN have been excluded as their MIR luminosities are not attributed to star forming activity, but to reprocessed higher frequency luminosity driven by the accretion on a super-massive black hole (10^8-10^{10} $M_\odot$). For the sake of comparison the estimates from the spectroscopic identifications in the HDF-S, and the HDF-N are shown. The ISOCAM observations of the HDF-S and HDF-N reach 15 μm fluxes down to $\sim$0.1 mJy (i.e., more than six times fainter than our survey) and probe a different region of the SFR vs. z plane. The shallower wide-area ELAIS survey is complementary to the deep surveys and is required to make a more accurate estimate of the SFR history of the Universe (see Pozzi et al. 2004). The ELAIS-S1 sources have mean SFRs of 13 $M_\odot$/yr, 45 $M_\odot$/yr and 242 $M_\odot$/yr, in the redshift ranges z<0.2, 0.2<z<0.4 and z>0.4 respectively. Obviously this should not be attributed to an evolutionary trend, but to the luminosity-redshift relation which is present in any flux limited sample like ELAIS-S1.

We have found a good correlation between the SFRs derived from the 15 μm luminosity and those derived from the 1.4-GHz luminosity (computed as $SFR[\frac{M_\odot}{yr}] = 1.1 \times 10^{-21}(\frac{\nu}{GHz})^\alpha L_{1.4GHz}[\frac{W}{Hz}]$, assuming a Salpeter IMF between 0.1 and 100 $M_\odot$, and a power-law spectrum with a spectral index $\alpha \sim 0.7$; $S_\nu \propto \nu^{-\alpha}$). The correlation between the SFRs obtained through the two different indicators reflects the radio-MIR luminosity correlation found for ELAIS-S1 galaxies by Gruppioni et al. (2003; see also Elbaz et al. 2002).

7. Summary

We have presented multiband (R, K, 1.4 GHz) and optical spectroscopic identifications of a reliable subsample of 406 15-μm sources from the ELAIS-S1 survey over the flux density range 0.5< $S_{15\mu m}$ <150 mJy. These observations substantially contribute to the understanding of the evolution of star-forming galaxies and AGN in the MIR, which is presented in two companion papers by Pozzi et al. (2004) and Matute et al. (in preparation) respectively. This paper has described the details of the ground-based follow-up observations and data reduction, and has presented optical identifications for $\sim$82% of the 15 μm sources down to R$\sim$23, and spectroscopic identification for $\sim$88% of the optically identified sample. The areal coverage and completeness of the survey has been described in detail, in order to allow statistical analyses. The source counts for star-forming galaxies and AGN have been derived: the ELAIS extragalactic sources down to $S_{15\mu m}$=0.6 mJy have a density of 370$\pm$14/deg^2, and produce a 15 μm background of $\nu I(\nu) = 0.34$ nW m^{-2}sr^{-1}. This corresponds to $\sim$12% of the total extragalactic background estimated by Metcalfe et al. (2003). Taking into account the optical based classification, we estimate an AGN contribution of at least $\sim$6% to the MIR sources brighter than $S_{15\mu m}$=0.6 mJy. A larger fraction is expected if the classification will be based on the X-ray luminosity. The line ratios of the optical spectra of the MIR galaxies suggest that they are affected by substantial reddening, whith the more MIR-luminous sources having larger dust extinction. A general trend is found in the MIR-optical SEDs of *IRAS* and *ISO* galaxies whith the more MIR-luminous sources having larger L_{15}/L_R ratios. According to our analyses we conclude that most of the ELAIS galaxies fainter than R$\sim$23 should have redshift greater than 0.5 and are likely to be LIG-ULIG galaxies. As a consequence, the present sample of star-forming galaxies has to be considered virtually complete up to $z = 0.5$.

Based on observations collected at the European Southern Observatory, Chile, ESO N°: 57.A-0752, 58.B-0511, 59.B-0423, 61.B-0146, 62.P-0457, 67.A-0092(A), 68.A-0259(A), 69.A-0538(A), 70.A-0362(A); PATT proposal P076). This paper is based on observations with the Infrared Space Observatory (ISO). ISO is ane ESA project with instruments funded by ESA Member States (especially the PI countries: France,

Germany, the Netherlands and the United Kingdom) and with the partecipation of ISA and NASA. This research has made use of the NASA/IPAC Extragalactic Database (NED) which is operated by the Jet Propulsion Laboratory, California Institute of Technology, under contract with the National Aeronautics and Space Administration. This publication makes use of data products from the Two Micron All Sky Survey, which is a joint project of the University of Massachusetts and the Infrared Processing and Analysis Center/California Institute of Technology, funded by the National Aeronautics and Space Administration and the National Science Foundation. This research has been partially supported by ASI contracts ARS-99-75, ASI I/R/107/00, ASI I/R/113/01, MURST grants Cofin-98-02-32, Cofin-00-02-36. IM acknowledges a PhD grant from CNAA/INAF. DMA acknowledges the Royal Society for generous support. Ph. Héraudeau acknowledges the financial support provided through the European Community's Human Potential Programme under contract HPRN-CT-2002-00316, SISCO.

We wish to thank Lucia Pozzetti for interesting discussions, and the anonymous referee for the useful comments.

REFERENCES

Alexander, D.M., Aussel, H. 2000, Lecture Notes in Physics, 548, 113

Alexander, D.M., et al. 2001, ApJ, 554, 18

Alexander, D.M., Aussel, H., Bauer, F.E., Brandt, W.N., Hornschemeier, A. E., Vignali, C., Garmire, G.P., Schneider, D.P 2002, ApJ, 568, 85

Aussel, H., Césarsky, C.J., Elbaz, D., & Starck J.-L. 1999a, A&A, 342, 313

Aussel, H., Elbaz D., Césarsky, C.J., & Starck J.-L. 1999b, The Universe as seen by *ISO*, P. Cox & M.F. Kessler, ESA Special Publication series (SP-427), p. 1023

Bertin, E., Arnouts, S. 1996, A&AS, 117, 393

Bruzual, A.G., Charlot, S. 1993, ApJ, 405, 538

Cesarsky, C.J., et al. 1996, A&A, 315, L32

Chary, R., Elbaz, D., 2001, ApJ, 556, 562

Ciliegi, P., Zamorani, G., Hasinger, G., Lehmann, I., Szokoly, G., & Wilson G. 2003, A&A, 398, 901

Cohen, J.G., Hogg, D.W., Blandford, R., Cowie, L.L., Hu, E., Songaila, A., Shopbell, P., & Richberg K. 2000, ApJ, 538, 29

Dressler, A. et al. 1999, ApJS, 122, 51

Duc, P.A., et al. 2002, A&A, 382, 60

Elbaz, D., et al. 1999, A&A, 351, L37

Elbaz, D., et al. 2002, A&A, 384, 848

Elvis, M., et al. 1994, ApJS, 95, 1

Fadda, D.Flores, H., Hasinger, G., Franceschini, A., Altieri, B., Cesarsky, C.J., Elbaz, D., Ferrando, Ph. 2002, A&A, 383, 838

Fixsen, D.J., Dwek, E., Mather, J.C., Bennett, C.L., & Shafer R.A. 1998, ApJ, 508, 123

Fiore F., et al. 2000, New Ast., 5, 143

Fiore F., et al. 2003, A&A, 409, 79

Flores, H., et al. 1999, ApJ, 517, 148

Förster Schreiber, N.M., Sauvage, M., Charmanfaris, V., Laurent, O., Gallais, P., Mirabel, I.F., & Vigoux, L. 2003, A&A, 399, 833

Franceschini, A., et al. 2003, A&A, 403, 501

Gruppioni, C., et al. 1999, MNRAS, 305, 297

Gruppioni, C., Lari, C., Pozzi, F., Zamorani, G., Franceschini, A., Oliver, S., Rowan-Robinson, M. & Serjeant, S. 2002, MNRAS, 335, 831

Gruppioni, C., Pozzi, F., Zamorani, G., Ciliegi, P., Lari, C., Calabrese, E., La Franca, F., Matute, I. 2003, MNRAS, 341, L1

Hamuy, M., et al. 1992, PASP, 104, 533

Hamuy, M., et al. 1994, PASP, 106, 566

Hauser, M.G., Arendt, R.G., & Kelsall, T. 1998, ApJ, 508, 25

Høg, E., et al. 2000, A&A, 355, L27

Hogg, D.W. , et al. 2000, ApJS, 127, 1

Kennicutt, R.C. 1992, ApJ, 388, 310

Kessler, M.F., et al. 1996, A&A, 315, 27

Lagache, G., Abergel, A., Boulanger, F., Désert, F.X., & Puget, J.-L. 1999, A&A, 344, 322

Landolt, A.U. 1992, AJ, 104, 340

Lari, C., et al. 2001, MNRAS, 325, 1173

Lemke, D., et al. 1996, A&A, 315, L64

Mann, R.G., et al. 2002, MNRAS, 332, 549

Matute, I., et al. 2002, MNRAS, 332, L11

Mazzei, P., Aussel, H., Xu, C., Salvo, M., De Zotti, G., & Franceschini, A. 2001, New Astronomy, 6, 265

Metcalfe, L., et al. 2003, A&A, 407, 791

Natali, F,, Giallongo, E., Cristiani, S., & La Franca, F. 1998, AJ, 115, 397

Oke, J.B. 1990, AJ, 99, 1621

Oliver, S., et al. 2000, MNRAS, 316, 749

Oliver, S., et al. 2002, MNRAS, 332, 536

Osterbrock D.E. 1989, Astrophysics of Gaseous Nebulae and Active Galactic Nuclei, Uni. Sci. Books

Poggianti, B.M., Smail, I., Dressler, A., Couch, W., Barger, A.J., Butcher, H., Ellis, R.S., & Oemler, A. 1999, ApJ, 529, 157

Poggianti, B.M., & Wu, H. 2000, ApJ, 529, 157

Pozzi, F., et al. 2003, MNRAS,343, 1148

Pozzi, F., et al. 2004, ApJ, in press [astro-ph/0403242]

Puget, J.L., Arbergel, A., Bernard, J.P., Boulanger, F., Burton W.B., Desert, F.X., & Hartmann, D. 1996, A&A, 308, L5

Rowan-Robinson M., et al. 2004, MNRAS, in press [astro-ph/0308283]

Rush, B., Malkan, M.A., & Spinoglio, L. 1993, ApJS, 89, 1

Salpeter, E.E. 1955, Vistas in Astronomy, 1, 283

Silva, L., Granato, G.L., Bressan, A., & Danese, L. 1998, ApJ, 509, 103

Sturm, E., Lutz, D., Tran, D., Feuchtgruber, H., Genzel, R., Kunze, D., Moorwod, A.F.M., Thornley, M.D., 2000, A&A, 358, 481

Sutherland, W., & Saunders W. 1992, MNRAS, 259, 413

Tresse, L., Rola, C., Hammer, F., Stasinska, G., Le Fevre, O., Lilly, S.J., Crampton, D. 1996, MNRAS, 281, 847

Väisänen, P., et al. 2002, MNRAS, 337, 1043

Veilleux, S., & Osterbrock, D.E. 1987, ApJS, 63, 295

This preprint was prepared with the AAS LaTeX macros v5.0.

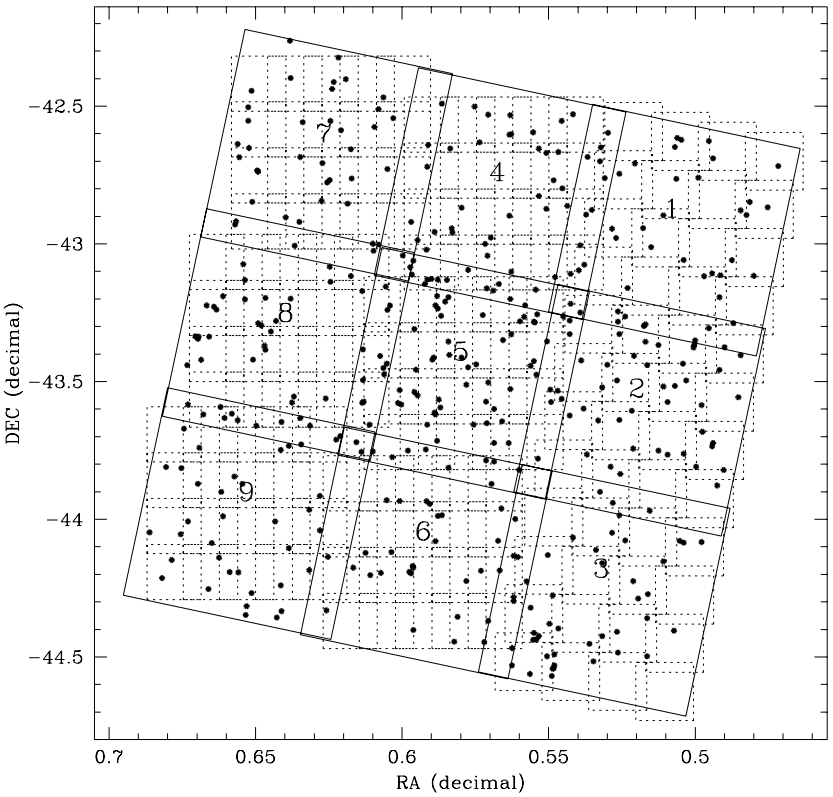

Fig. 1.— ELAIS-S1 field divided into the 9 ISOCAM rasters. The total area is 4.2 deg^2. The numbers refer to the individual rasters. The 168 CCD pointings and the 406 ELAIS-S1 sources are shown by dotted lines and filled points, respectively.

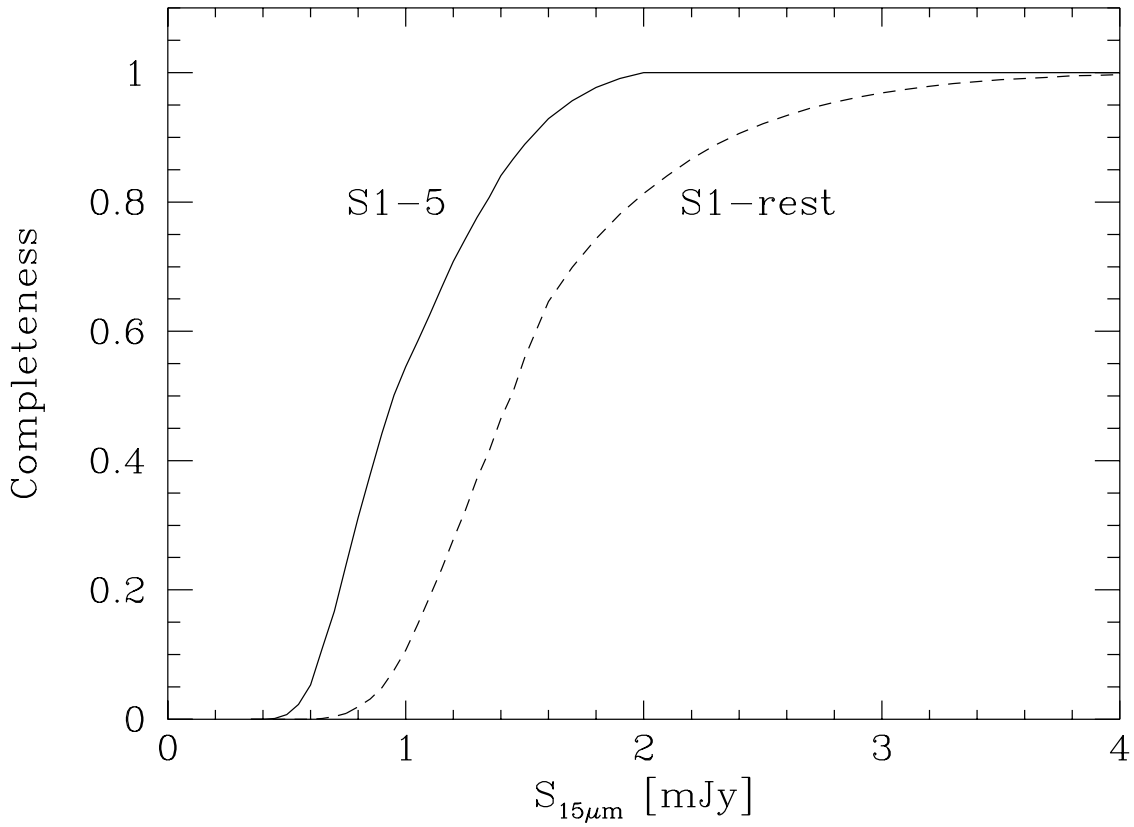

Fig. 2.— Completeness as a function of the 15 μm flux of the S1-5 (continuous line) and the S1-rest (dashed line) regions.

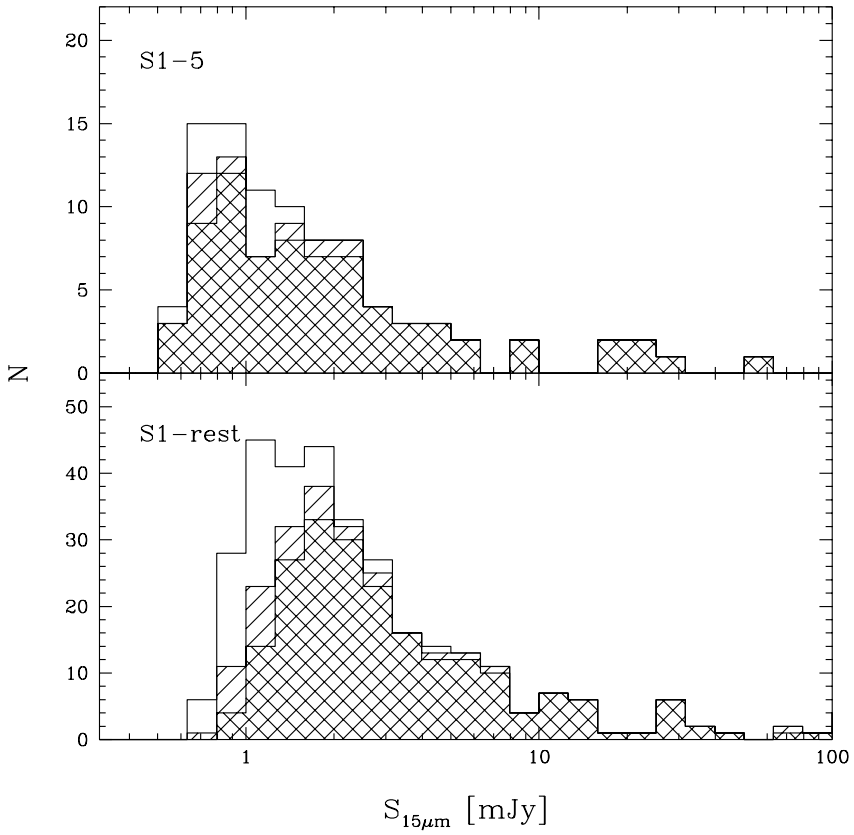

Fig. 3.— 15μm flux histograms of the 406 ELAIS-S1 sources in the S1-5 (*Top*) and S1-rest (*Bottom*) regions. The shaded histograms are the optically identified sources, and the cross-shaded histograms are the spectroscopically identified sources.

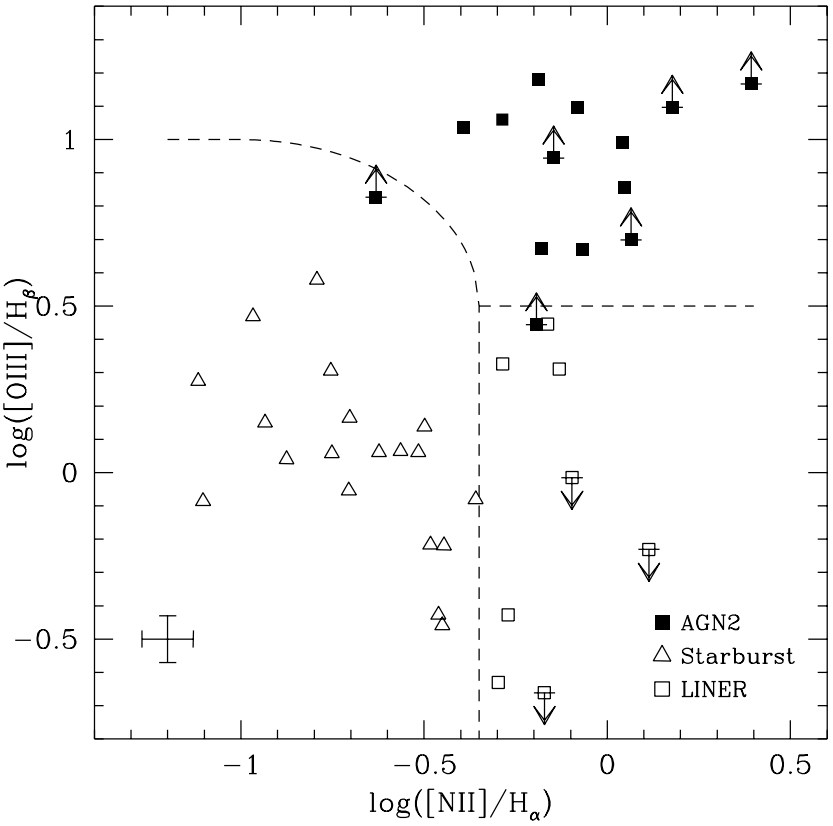

Fig. 4.— Diagnostic diagram for the classification of emission line galaxies. The dashed lines separate the regions of AGN2, LINERs and starburst galaxies (see e.g. Veilleux & Osterbrock 1987 and Tresse et al. 1996). The errorbars correspond to 10% uncertainties.

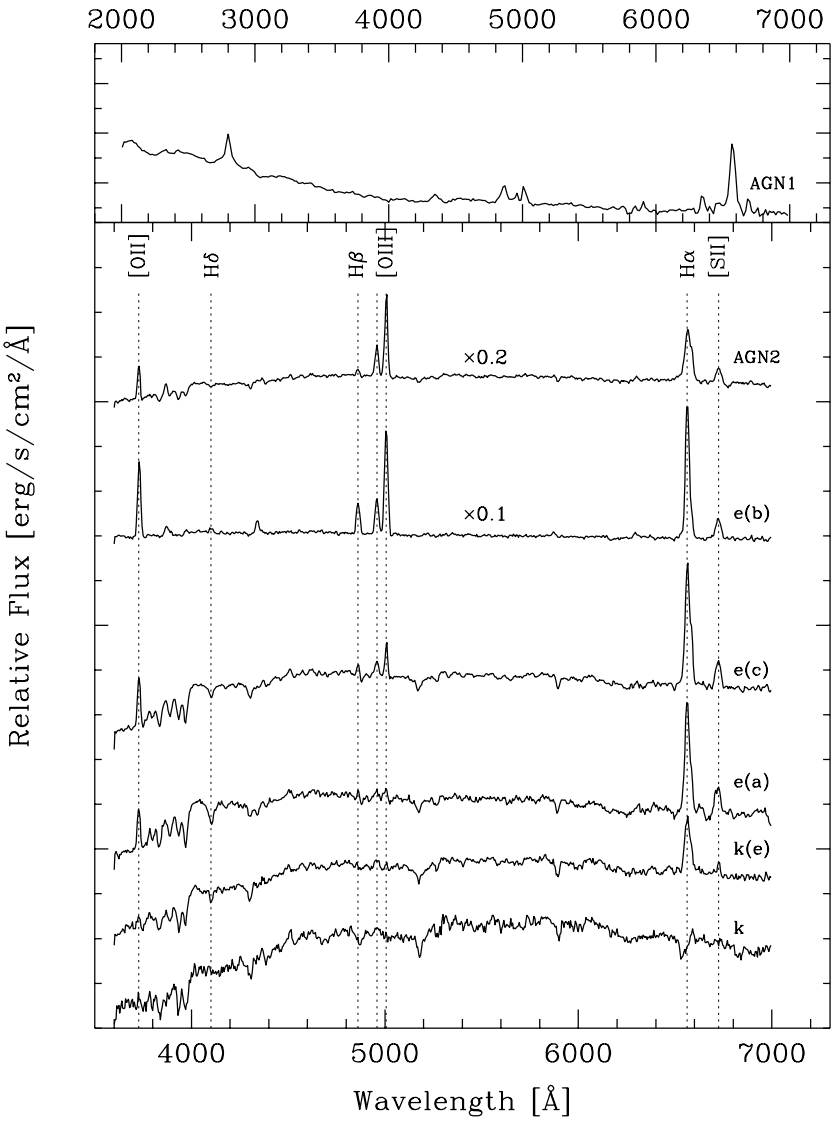

Fig. 5.— Composite spectra of the various type of galaxies classified in the ELAIS-S1 survey (see text).

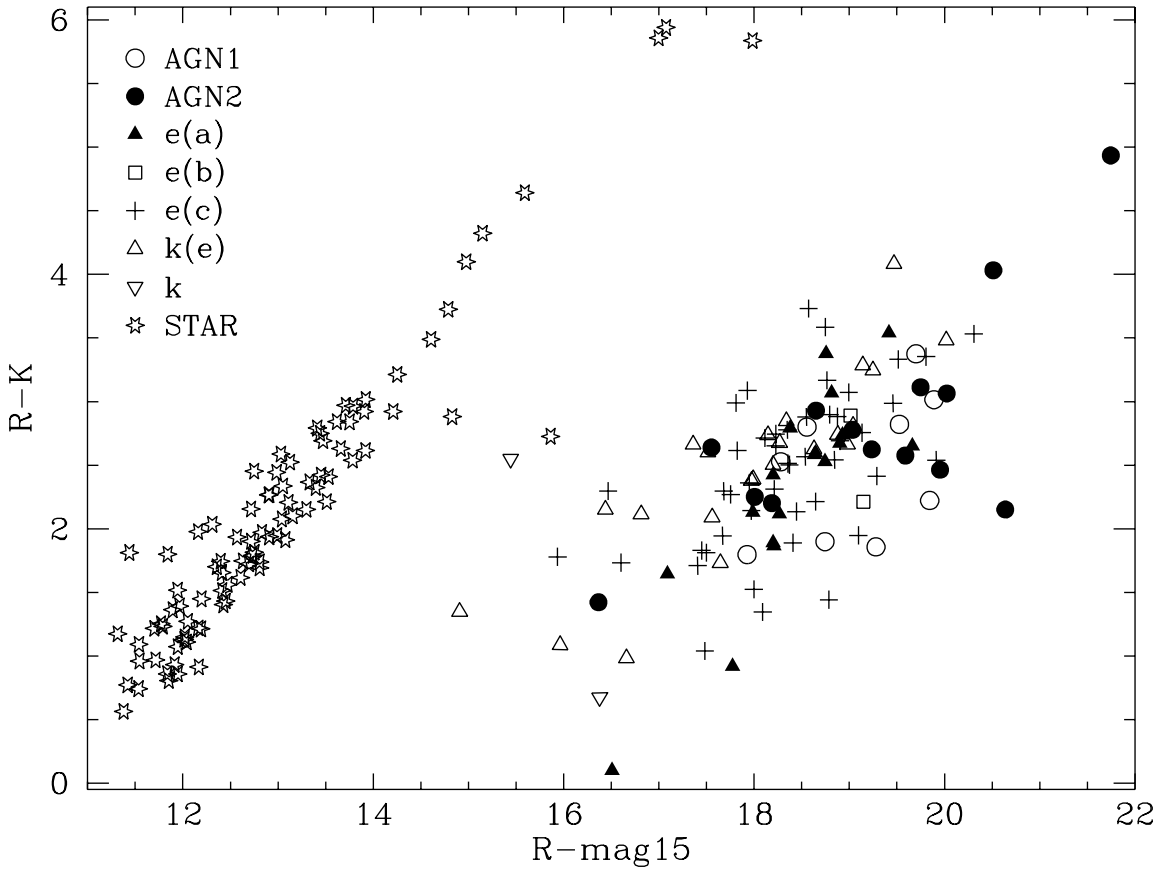

Fig. 6.— $R-K$ color versus $R-mag15$ color diagram of the 211 ELAIS-S1 sources detected both in the R and K bands. $mag15$ is a 15 μm magnitude computed as $mag15 = -2.5log(S_{15}(mJy))$.

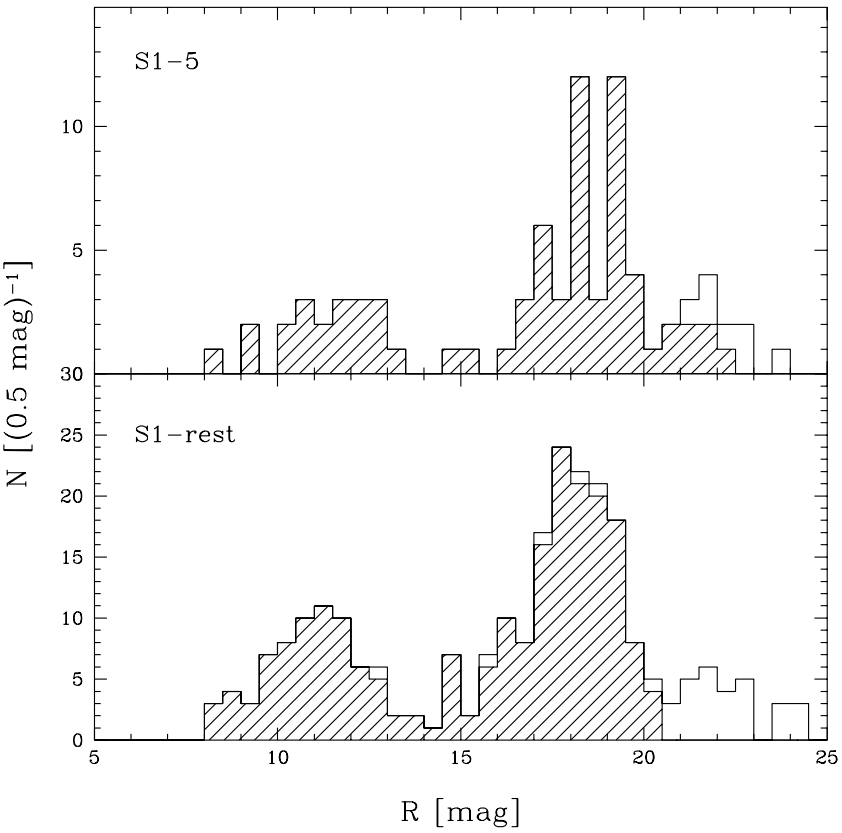

Fig. 7.— R-band magnitude histograms of the optically identified 15 μm sources in the S1-rest (*Top*) and S1-5 (*Bottom*) regions. The shaded histograms are the R-band distributions of the spectroscopically identified sources.

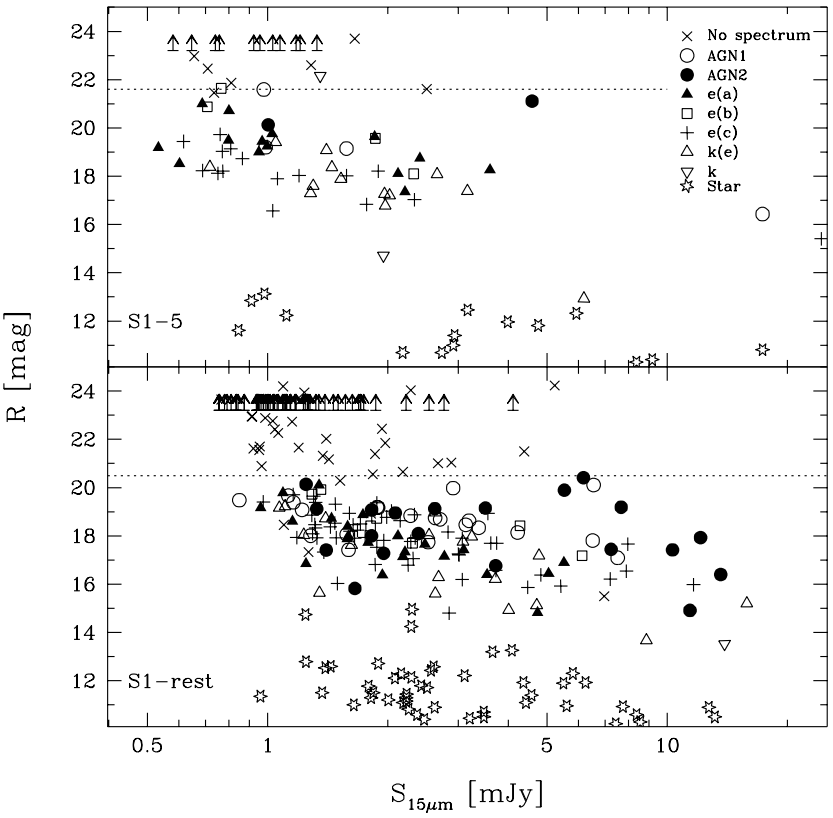

Fig. 8.— ELAIS-S1 spectroscopically identified sources in the $S_{15\mu m}$–R-band plane. *Upper panel:* sources in the S1-5 area. *Lower panel:* sources in the S1-rest area. The dashed lines are the optical limits of the spectroscopically complete samples (see §4.3), while the upper arrows are sources without optical counterpart on CCDs.

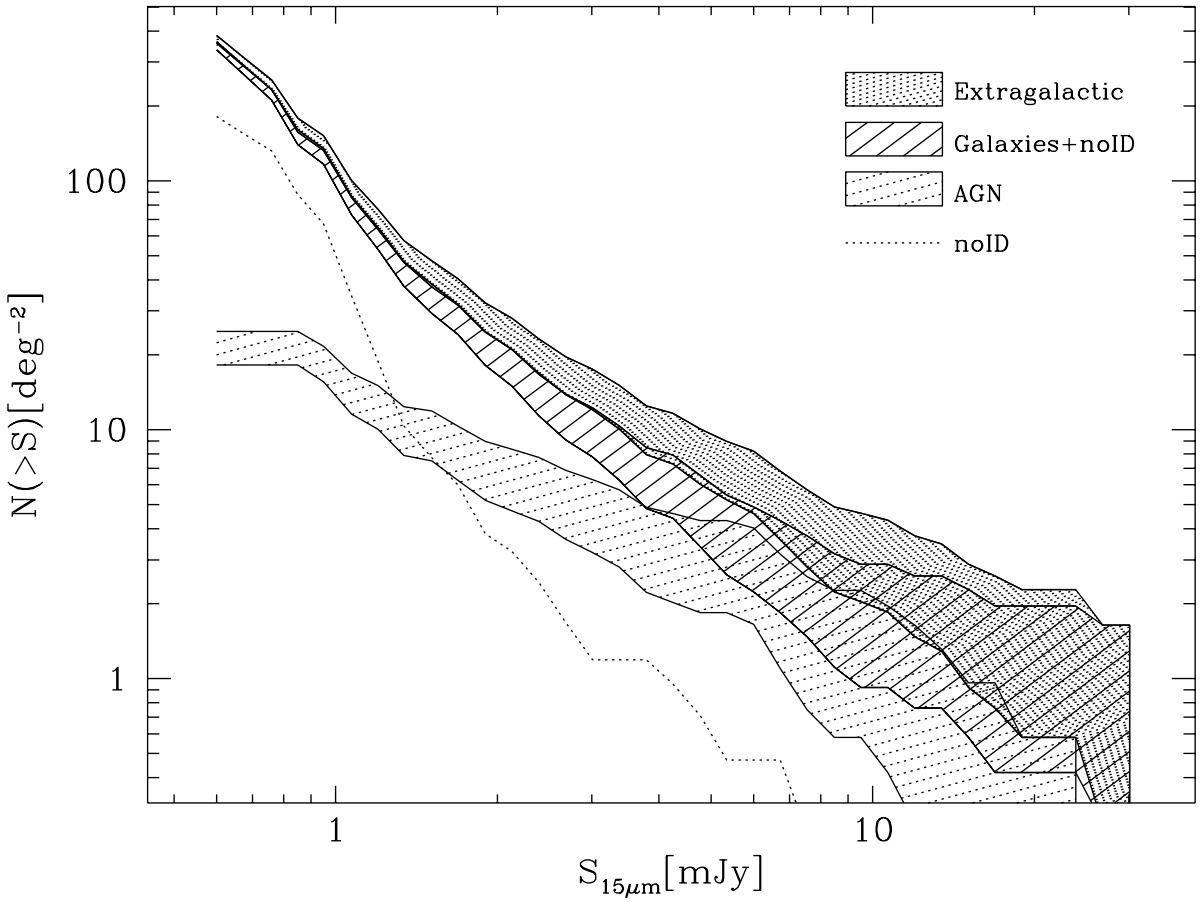

Fig. 9.— Integral counts from the ELAIS-S1 survey for a) all the extragalactic sources, b) the galaxies plus the no identified sources which are assumed to be galaxies, c) the AGNs and d) the no identified sources. The counts of galaxies and AGN corrected for the contribution of X-ray emitting AGNs are also shown. The no identified sources (*noIDs*) includes 72+2 EMPTY sources plus 40 (mainly faint: 20.5<R<23.3) sources without redshift. Errors are at the 1σ confidence level, based on Poisson statistic.

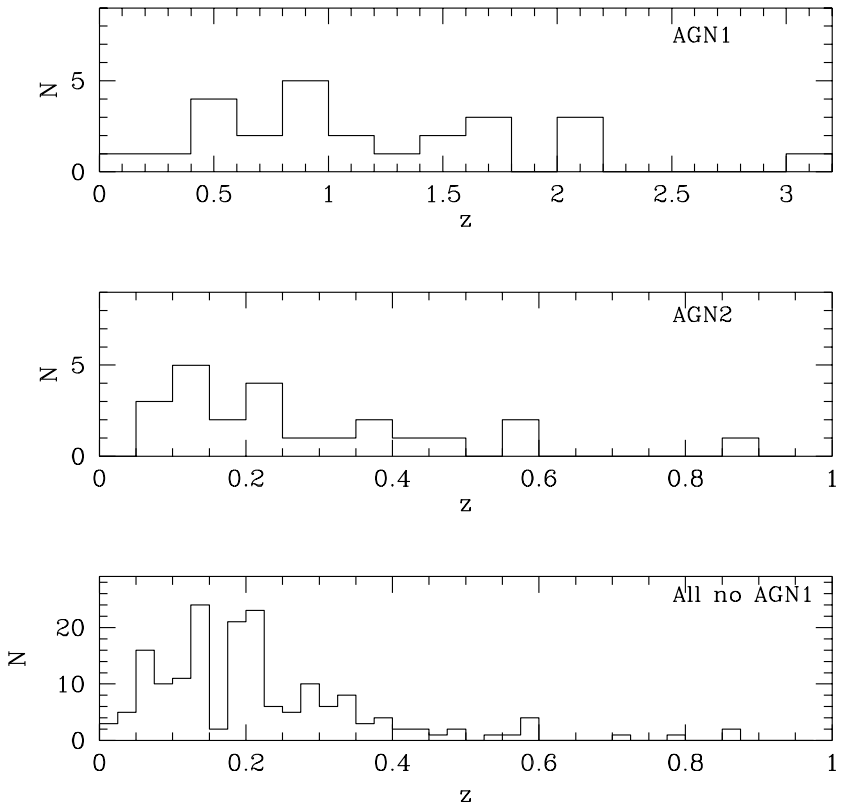

Fig. 10.— Redshift distributions of the spectroscopically identified sources in ELAIS-S1. *Top*: AGN1; *Middle*: AGN2; *Bottom*: all the extragalactic sources which are not AGN1.

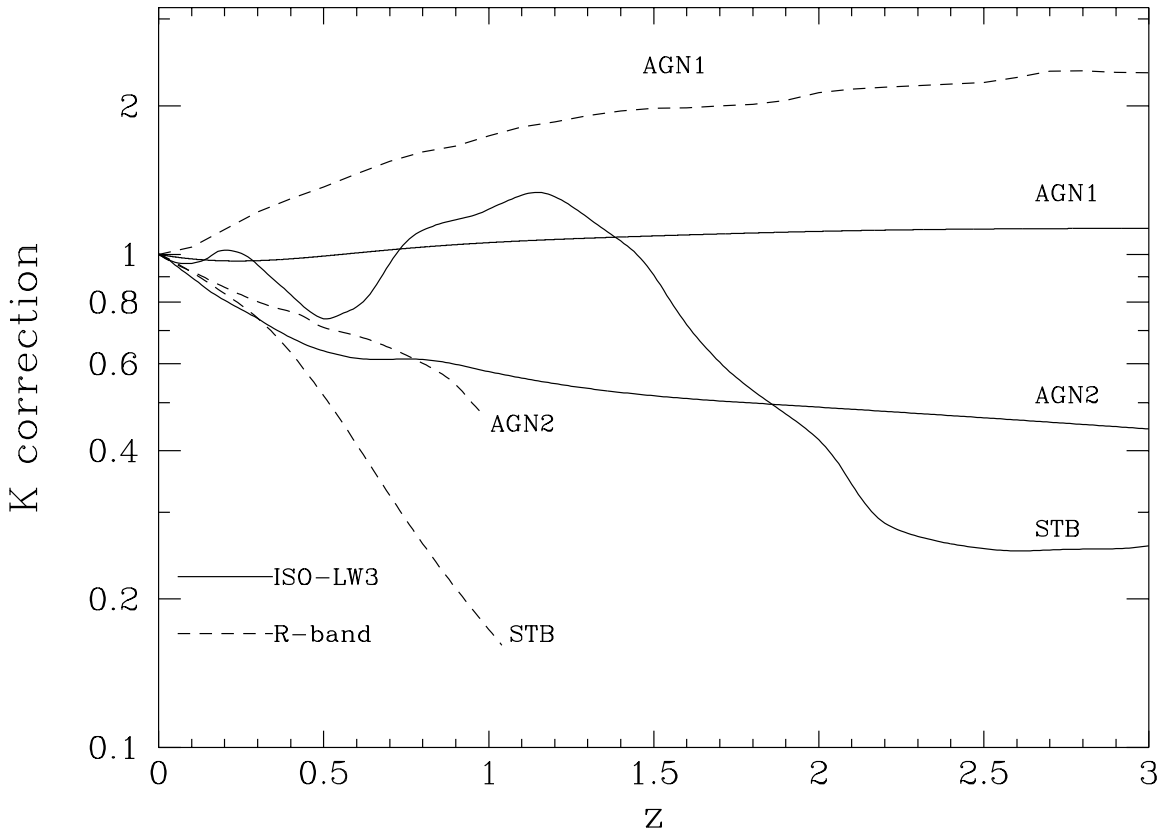

Fig. 11.— K-correction (log(S(z)/S(0))) in the ISOCAM-LW3 15 μm and R-band filters for type 1 AGN, type 2 AGN and Starburst galaxies. For Starburst galaxies the MIR K-correction with M82 is shown as it is used in the vast majority of the cases (see §6.1).

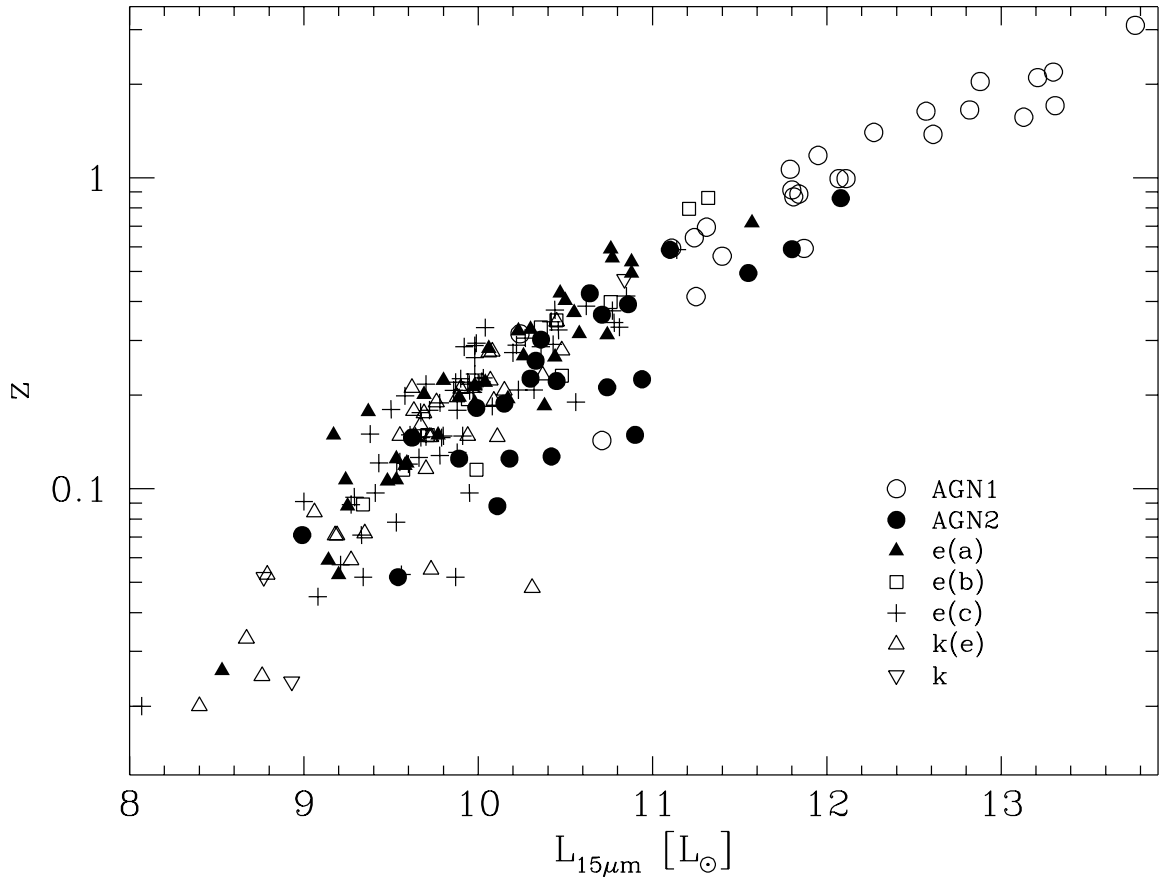

Fig. 12.— Luminosity at 15 μm of the ELAIS-S1 spectroscopically identified sources as a function of redshift.

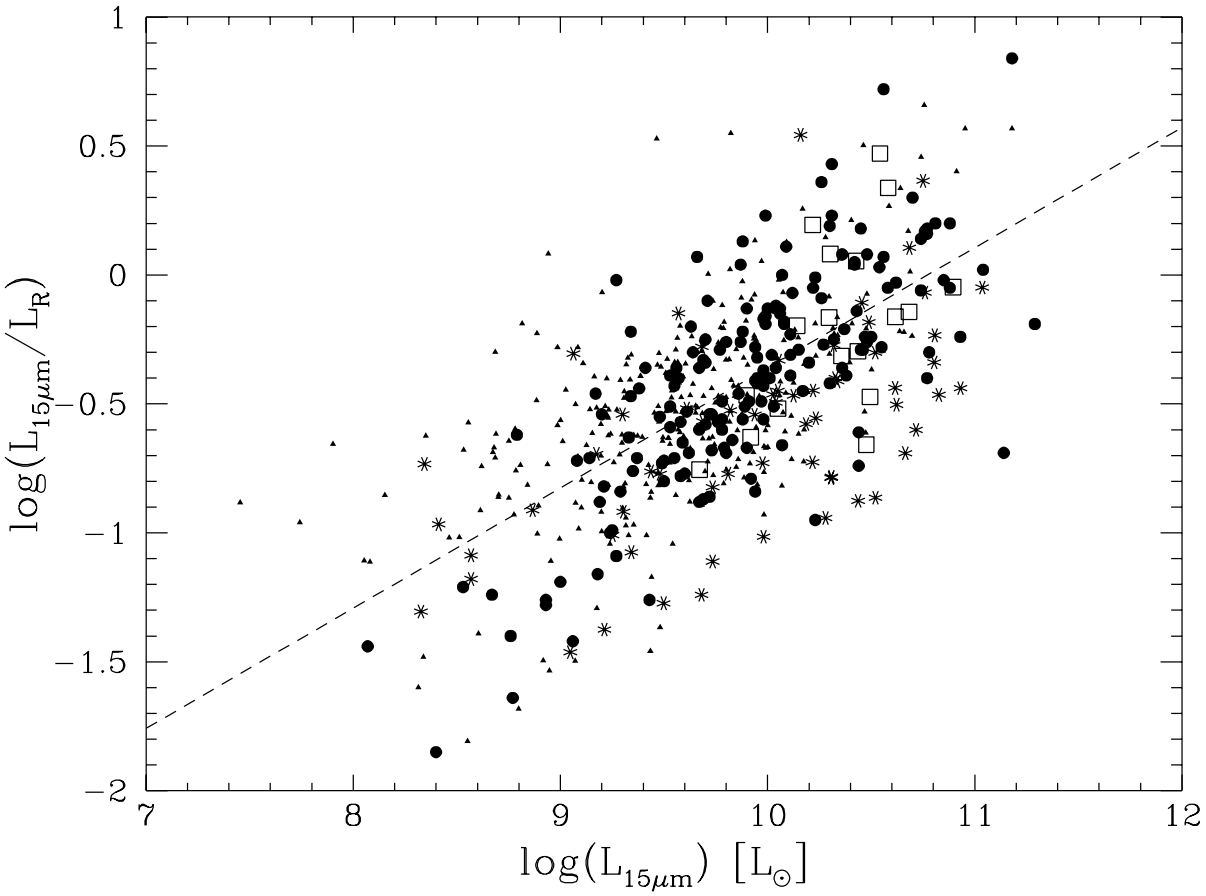

Fig. 13.— L_{15}/L_R ratio as a function of L_{15} for different MIR surveys. Filled circles are the ELAIS-S1 sample; open squares and asterisks are data from HDF-S and HDF-N, respectively; filled triangles are *IRAS* galaxies from Rush, Malkan and Spinoglio (1993). Type 1 AGN have been excluded, due to the different mechanism responsible for their luminosities.

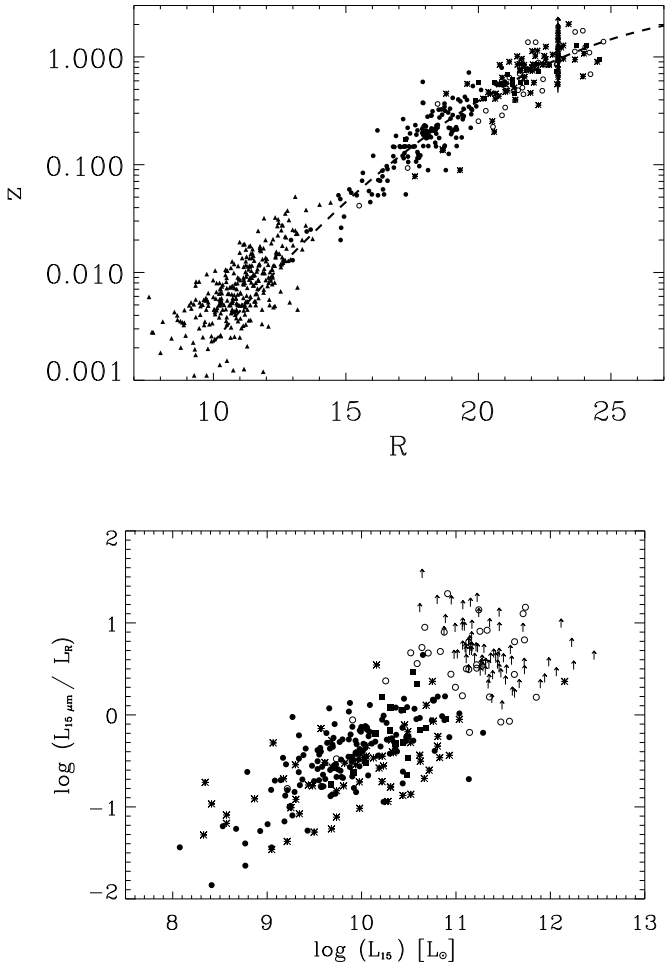

Fig. 14.— *Top*: $R - z$ plane with the lower limits estimates of the redshift for the *noIDs* sources as described in §6.3. Filled circles are ELAIS-S1 data points; filled squares, asterisks and filled triangles are data from HDF-S, HDF-N and RMS respectively. ELAIS-S1 sources with optical counterparts, but lacking redshift information are shown as open circles, while empty fields are represented as pointed-up arrows (all at $R = 23$). The dashed line is the best-fitting polynomial function used for estimating redshifts for sources without spectroscopic identification. *Bottom*: Same as in figure 13, but with also the lower limits for the *noIDs* sources shown. Symbols are the same as in the *top* panel. Data from RMS are not shown in this plot for greater clarity.

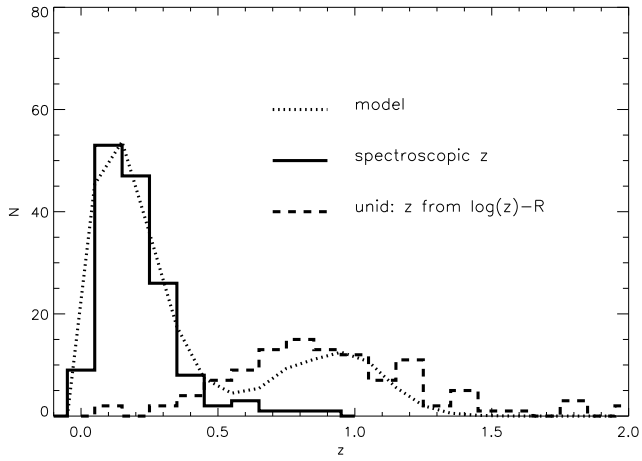

Fig. 15.— Measured redshift distribution for the spectroscopically identified sources in S1 (solid histogram) and estimated redshift distribution for the unidentified ones (dashed histogram). Data are compared with the prediction of the model derived from the 15 μm luminosity function obtained from our data and fitting the source counts (see Pozzi et al. 2004), shown as dotted line.

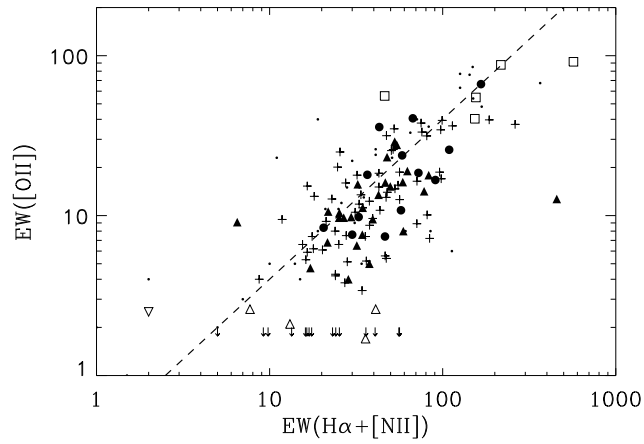

Fig. 16.— EW of [OII] versus EW of Hα+[NII] for ELAIS-S1 sources (symbols as in Figure 6), and 39 *IRAS* galaxies from Rush, Malkan & Spinoglio (1993, small dots), using data from literature. The pointed-down arrows are sources with Hα+[NII] measurement but no [OII] detected. The dashed line shows the relation $EW([OII]) = 0.4EW(H\alpha + [NII])$ found by Kennicutt (1992) for local field galaxies (see §6.4).

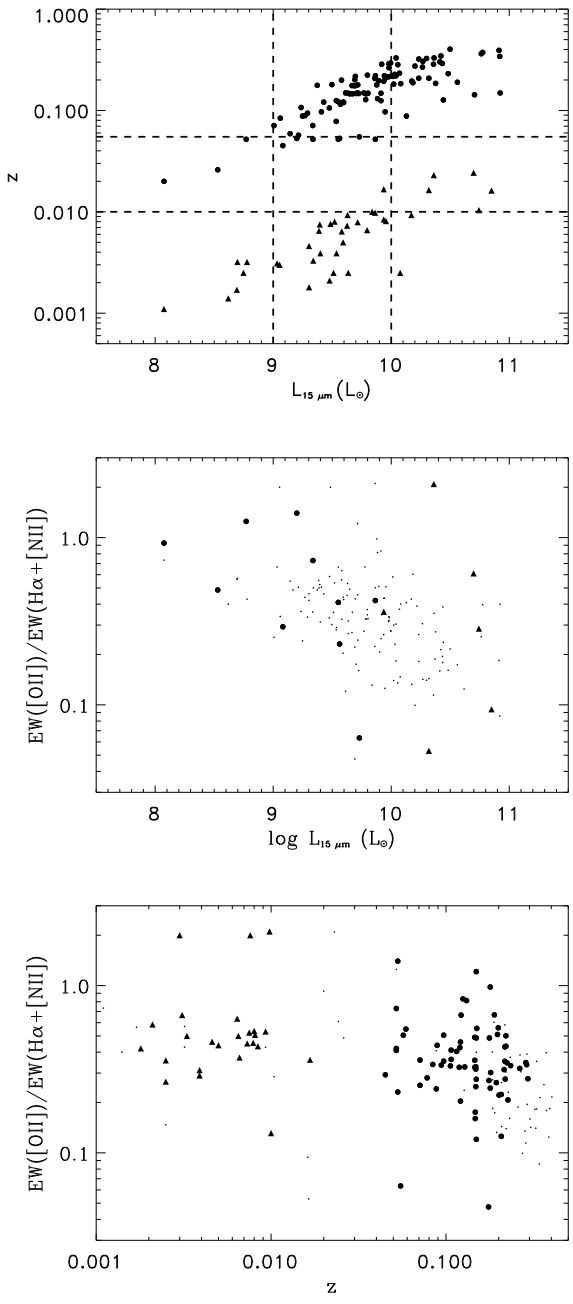

Fig. 17.— *Top* - Luminosity-redshift distribution of the ELAIS-S1 galaxies (filled circles) plus 39 *IRAS* galaxies from RMS (triangles). Dashed lines show the regions selected for disentangling the luminosity/redshift dependence of the reddening (see §6.4). *Middle* - $EW([OII])/EW(H\alpha+[NII])$ ratio versus 15 μm luminosity for the galaxies with $0.010<z<0.055$ (symbols as above). *Bottom* - $EW([OII])/EW(H\alpha+[NII])$ ratio versus redshift for the galaxies with $9 < logL_{15}(L_{\odot}) < 10$ (symbols as above). The remaining ELAIS-S1 plus RMS galaxies are represented with small filled circles.

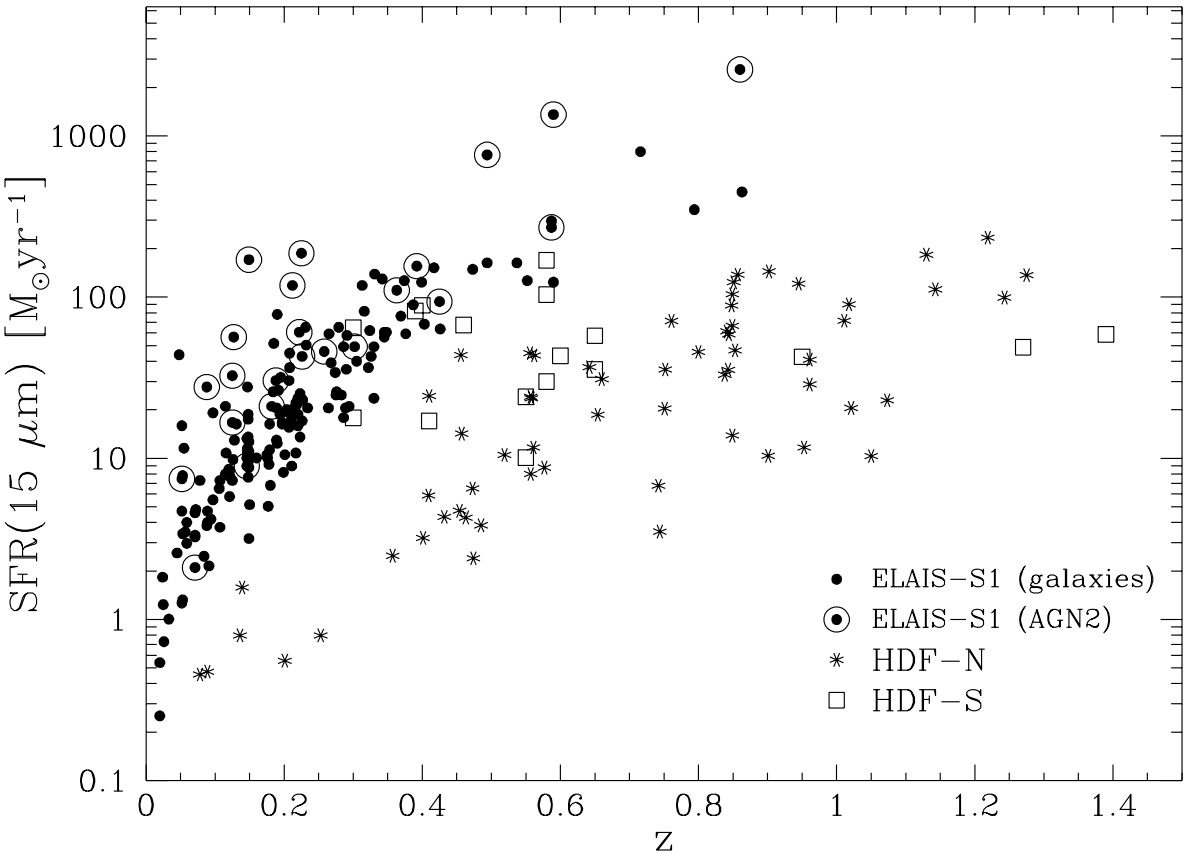

Fig. 18.— Rates of the star formation based on the estimates of the MIR (15 μm) luminosity, as a function of redshift. Type 1 AGN have been excluded as their MIR luminosity is not attributed to the star forming activity.

Table 1. The completeness function of S1-5 and S1-rest

Flux	S1-5	S1-rest
0.45	0.001	0.000
0.50	0.007	0.000
0.55	0.023	0.000
0.60	0.053	0.000
0.65	0.110	0.001
0.70	0.167	0.004
0.75	0.239	0.009
0.80	0.312	0.019
0.85	0.379	0.031
0.90	0.442	0.049
0.95	0.501	0.076
1.00	0.545	0.107
1.05	0.585	0.147
1.10	0.625	0.189
1.15	0.668	0.232
1.20	0.708	0.278
1.25	0.743	0.323
1.30	0.776	0.373
1.35	0.807	0.415
1.40	0.841	0.465
1.45	0.866	0.506
1.50	0.889	0.559
1.60	0.929	0.646
1.70	0.957	0.699
1.80	0.977	0.743
1.90	0.991	0.781
2.00	1.000	0.813
2.10	1.000	0.841
2.20	1.000	0.867
2.30	1.000	0.888
2.40	1.000	0.906
2.50	1.000	0.921
2.60	1.000	0.934
2.70	1.000	0.945
2.80	1.000	0.954
2.90	1.000	0.962
3.00	1.000	0.969
3.10	1.000	0.974
3.20	1.000	0.979
3.30	1.000	0.983
3.40	1.000	0.986
3.50	1.000	0.989
3.60	1.000	0.991
3.70	1.000	0.993
3.80	1.000	0.995
3.90	1.000	0.996
4.00	1.000	0.997
4.10	1.000	0.999
4.20	1.000	1.000

Table 2. Sources in the ELAIS S1 Sample

Name (1)	# (2)	F_{15} (3)	α_O (J2000) (4)	δ_O (J2000) (5)	Off (6)	R (7)	K (8)	Lik (9)	Rel (10)	$F_{1.4}$ (11)	z (12)	Cl (13)	L_{15} (14)	L_R (15)	Notes (16)
ELAISC15_J003957-432013	8	3.01	00:39:57.85	-43:20:13.4	1.2	17.21	15.32	363.16	0.999	< 0.24	0.128	5	9.78	10.27	
ELAISC15_J003958-441511	9	25.39	00:39:58.67	-44:15:10.6	2.0	10.41	7.39	999.99	1.000	< 0.30	0.000	8	...	...	
ELAISC15_J004000-431325	8	1.01	...	...	...	...	...	...	...	...	...	0	...	...	
ELAISC15_J004004-433710	9	1.24	...	...	...	...	...	...	...	...	...	0	...	...	
ELAISC15_J004007-432516	8	3.11	00:40:06.88	-43:25:18.2	2.5	12.21	9.46	999.99	1.000	< 0.30	0.000	8	...	...	
ELAISC15_J004009-434424	9	2.62	00:40:09.26	-43:44:25.3	0.9	19.13	...	97.33	0.997	< 0.30	0.188	2	10.15	9.87	
ELAISC15_J004010-432012	8	1.03	...	...	...	...	...	...	...	...	...	0	...	...	

Note. — The complete version of this table is in the electronic edition of the Journal. The printed edition contains only a sample. The columns are as follows: (1) Name of the 15-μm source as in Lari et al. (2001). (2) Raster number. (3) The 15-μm flux in mJy units. (4-5) The ra and dec of the optical counterpart, J2000. (6) Offset of the optical counterpart from the 15-μm source position in arcsec units. (7-8) The R and K band Vega magnitudes. (9) Likelihood of the optical identification; 999.99 was assigned to stars (see §3.2). (10) Reliability of the optical identification (see §3.2). (11) 1.4 GHz flux or 3σ upper limit in mJy units. (12) Redshift. (13) Spectroscopic class where: 0 means no spectra available, 1 is AGN1, 2 is AGN2, 3 is e(a) galaxy, 4 is e(b) galaxy, 5 is e(c) galaxy, 6 is k(e) galaxy, 7 is k galaxy and 8 is star. An L is appended for objects classified LINERS according to the line ratios diagnostics (see §4.2). (14) $\log(\nu L\nu)$ 15-μm luminosity in solar units. (15) $\log(\nu L\nu)$ R band luminosity in solar units. (16) Notes, O is for outside CCD observations, M is for multiple optical counterparts, and B for Broad Absorption Line (BAL) QSO.

Table 3. Rest frame line measurements

Name (1)	F_{15} (2)	z (3)	Cl (4)	D_{4000} (5)	EW([OII]) (6)	EW(Hδ) (7)	EW(Hβ) (8)	EW([OIII]) (9)	EW(Hα) (10)	EW([NII]) (11)	EW([SII]) (12)
ELAISC15_J002904-432415	1.61	0.207	5	1.20	-8.9	3.1	-3.7	0.0	-56.7	-10.6	-12.0
ELAISC15_J002915-430333	2.04	0.417	5	1.23	-39.2	3.4	-10.3	-13.9	...	...	...
ELAISC15_J002924-432233	2.34	0.374	5L	1.17	-39.4	0.0	-3.4	0.0	-36.4	-47.3	-46.3
ELAISC15_J002939-430625	3.73	0.071	5	1.22	-11.8	3.6	-1.9	0.0	-22.7	-8.6	-8.4
ELAISC15_J002949-430703	1.33	0.302	2	1.40	-7.4	0.0	0.0	-25.0	-15.8	-23.8	-12.9
ELAISC15_J003001-432202	1.47	0.274	5	1.33	-3.4	3.4	0.0	0.0	-28.1	-8.0	0.0
ELAISC15_J003011-432947	1.35	0.084	6	1.87	-2.6	0.0	-1.1	0.0	-4.8	-3.4	0.0

Note. — The complete version of this table is in the electronic edition of the Journal. The printed edition contains only a sample. The columns are as follows: (1) Name of the 15-μm source as in Lari et al. (2001). (2) The 15-μm flux in mJy units. (3) Redshift. (4) Spectroscopic class as in Table 2. (5) Calcium break. (6-12) Rest frame EW in Å units of the [OII]λ3727, Hδ, Hβ, [OIII]λ5007, Hα, [NII]λ6583, and [SII]λ6725 lines; positive values mean absorption.

Table 4. The integral extragalactic counts at 15 μm

S_{15} (mJy)	All (N(>S)/deg^2)	Galaxies[a] (N(>S)/deg^2)	AGN1+AGN2[b] (N(>S)/deg^2)	AGN1 (N(>S)/deg^2)	AGN2[b] (N(>S)/deg^2)
0.60	370±14	349 ±13	21.5±3.3	13.6 ±2.6	7.9 ±2.0
0.76	242±11	221 ±10	21.5±3.3	13.6 ±2.6	7.9 ±2.0
0.95	140.8±8.4	122.2 ±7.8	18.6±3.1	10.7 ±2.3	7.9 ±2.0
1.20	70.1±5.9	57.6 ±5.4	12.5±2.5	6.1 ±1.7	6.4 ±1.8
1.51	42.4±4.6	32.7 ±4.0	9.7±2.2	4.8 ±1.6	4.9 ±1.6
1.90	22.8±3.7	20.7 ±3.2	7.1±1.9	3.2 ±1.3	3.9 ±1.4
2.39	19.3±3.1	13.3 ±2.6	6.0±1.7	2.9 ±1.2	3.1 ±1.2
3.01	14.1±2.7	9.3 ±2.2	4.8±1.5	1.9 ±1.0	2.9 ±1.2
3.79	9.5±2.2	5.9 ±1.7	3.6±1.3	1.2 ±0.8	2.4 ±1.1
4.77	7.3±1.9	4.3 ±1.5	3.1±1.2	1.0 ±0.7	2.1 ±1.0
6.00	5.7±1.7	2.8 ±1.2	2.8±1.2	1.0 ±0.7	1.8 ±1.0
7.55	3.6±1.3	1.90±0.97	1.7±0.9	...	1.4 ±0.8
9.51	2.6±1.1	1.19±0.77	1.4±0.8	...	1.2 ±0.8
11.97	1.9±1.0	0.95±0.69	1.0±0.7	...	...
15.07	1.19±0.77	0.71±0.60	...	...	...
18.98	0.71±0.60	0.48±0.49	...	...	...

[a] Including sources without spectroscopic classification (*noIDs*).

[b] These values should be considered lower limits (see §4.2 and §5).

Table 5. Mean E(B-V)

Class	E(B-V)
e(b).....	0.43-0.52
e(c).....	0.82-1.59
e(a).....	1.02-1.42
k(e).....	0.64-1.87